

GROWTH AND DOPING OF NOVEL TL-CONTAINING III-V MATERIAL
SYSTEMS USING GAS-SOURCE MOLECULAR BEAM EPITAXY

By

MICHAEL J. ANTONELL

A DISSERTATION PRESENTED TO THE GRADUATE SCHOOL
OF THE UNIVERSITY OF FLORIDA IN PARTIAL FULFILLMENT
OF THE REQUIREMENTS FOR THE DEGREE OF
DOCTOR OF PHILOSOPHY

UNIVERSITY OF FLORIDA

1997

ACKNOWLEDGMENTS

The author would like to thank his supervisory committee chairperson, Dr. C.R. Abernathy, for providing guidance and support that have made his studies here at UF rewarding and enjoyable. The advice and support from the other members of this committee, specifically, Dr. S.R. Bates, Dr. K.S. Jones, Dr. S.J. Pearton, and Dr. F. Sharifi, is also greatly appreciated. The author is grateful to Dr. Abernathy, Dr. Holloway and Dr. Jones for giving him the opportunity to come to the University of Florida and for helping him make a modest but adequate living while continuing his education.

The author would also like to acknowledge the Air Force Office of Scientific Research (AFOSR) for the support of this research under grant numbers F49620-1-0001 and F49620-96-1-0364. Special thanks to SRI Int. specifically A. Sher, M. Berding, M. van Schilfgaarde, S. Krishnamurthy, and K. Sabo for providing the TI model and working with the author to improve it.

The author wishes to thank his family, especially his parents, whose unselfish sacrifices and support throughout his life are greatly appreciated. Special thanks go to friends who have supported the author throughout all of his life, namely, Grant Cook and Andy Jozwiak, and throughout his undergraduate schooling, Dr. Richard Jones and Terry Fullum. Thanks to Mr. and Mrs. John Cook for treating him like one of the family for 25 years and counting. Thanks to the author's "Pa", Wayne Acree, for everything from microprobe and SEM instruction to at least 10 pounds! Thanks to all friends here at UF, especially Sushil and Wish for always helping out when needed, Winston for being a good

friend and a great guy to work with, and everyone else like Steve, Rob, Brent, Jesse, Mike, Jay, Matt, JV, Sean, Cathy, and the many who are not listed but deserve to be.

Thanks to Chris Santana for lots of stuff, too much to mention and Jeff Trexler for a lot of fun and road trips (The Final Four, no really... Florida actually made it once). Finally, thanks to Gator sports and athletes that gave the author something to do (other than work) like watching games or the author's hobby, photography.

The author's father was right when he said: "When you finish and all things are considered, you will only remember the good times you had and the good friends you made." Thanks for all those years of good advice.

TABLE OF CONTENTS

ACKNOWLEDGEMENTS.....	ii
ABSTRACT.....	vi
CHAPTERS	
1. INTRODUCTION	1
1.1 Motivation and Objectives	1
1.2 Background Information	3
1.2.1 Theoretical Predictions and Calculations	3
1.2.2 Previous Experimental Work on Tl Containing Materials	6
1.2.3 Summary	8
1.3 Scope of the Present Work	10
2. EXPERIMENTAL.....	14
2.1 Description of the Growth Process	14
2.1.1 Gas Source Molecular Beam Epitaxy	14
2.2 Mechanisms of Epitaxial Growth	18
2.3 Dopant Sources	20
2.3.1 Growth and Characterization of Te-doped InP	20
2.3.2 Growth and Characterization of C-doped InSb	21
2.4 Source Chemistry	22
2.4.1 Group III Sources	22
2.4.2 Group V Sources	24
2.5 Solubility and Segregation	25
2.6 Safety Issues	26
2.7 Characterizational Techniques	27
2.7.1 Sample Handling and Storage	28
2.7.2 X-ray Diffraction	29
2.7.2.1 Powder x-ray diffraction	29
2.7.2.2 High resolution x-ray diffraction	29
2.7.3 Electron Microprobe	32
2.7.4 Auger Electron Spectroscopy	32
2.7.5 Scanning Electron Microscopy	33
3. THE THALLIUM CONTAINING PHOSPHIDE SYSTEM	45
3.1 Introduction	45
3.2 The Binary Tl-P Material System	46
3.2.1 The Growth of Tl-P Compounds	47
3.2.2 Closed Space Vapor Transport	48
3.2.3 Summary of the Tl-P Synthesis	48
3.3 Synthesis of Compounds Containing Indium, Thallium and Phosphorus	49

3.3.1 Efforts to Suppress Droplet Formation	50
3.3.2 Comparison of InTlP with Published Results	51
3.4 Summary of the InTlP Ternary Alloy System	53
4. THE THALLIUM CONTAINING ARSENIDE SYSTEM	64
4.1 Introduction	64
4.2 The Growth of Tl-As Compounds	65
4.3 Summary of the Tl-As Binary Alloy	66
4.4 Indium, Thallium and Arsenic Containing Ternary Alloys	67
4.5 Summary of the InTlAs Ternary Alloy System	70
4.6 Modification of Tl-containing Phosphide and Arsenide Theory.....	70
5. THE THALLIUM CONTAINING ANTIMONIDE SYSTEM.....	81
5.1 Introduction.....	81
5.2 The Growth of Tl-Sb Compounds	83
5.3 Summary of the Tl-Sb Binary System	85
5.4 Indium, Thallium and Antimony Containing Ternary Compounds.....	86
5.5 Summary of the InTlSb Ternary Compounds.....	87
5.6 Modification of Theory Based on Antimonide Experimental Data.....	88
5.7 Segregation Theory Pertaining to the Tl Containing III-V Materials	88
6. N-TYPE DOPING OF III-V MATERIALS	98
6.1 Introduction	98
6.2 Incorporation Characteristics of TlPIn-DIPTe	99
6.3 Thermal Stability of Te Doped InP.....	102
6.4 Conclusions	104
7. P-TYPE DOPING OF III-V MATERIALS	119
7.1 Introduction.....	119
7.2 Incorporation Characteristics of Carbon Tetrabromide	121
7.3 The Behavior of C in III-V Materials	123
7.4 Conclusions.....	124
8. CONCLUSIONS AND FUTURE RECOMENDATIONS	134
8.1 Conclusions	134
8.2 Future Recommendations.....	137
LIST OF REFERENCES	138
BIOGRAPHICAL SKETCH	143

Abstract of Dissertation Presented to the Graduate School
of the University of Florida in Partial Fulfillment of the
Requirements for the Degree of Doctor of Philosophy

GROWTH AND DOPING OF NOVEL TL-CONTAINING III-V MATERIAL SYSTEMS
USING GAS-SOURCE MOLECULAR BEAM EPITAXY

By

Michael J. Antonell

August 1997

Chairperson: Dr. Cammy R. Abernathy

Major Department: Materials Science and Engineering

The growth, doping and characterization of the Tl- and InTl-containing material systems have been attempted using gas-source molecular beam epitaxy (GSMBE) using a combination of elemental group III sources and elemental and precracked gaseous group V sources. Tl was found to incorporate to an atomic fraction $<1\%$ in the phosphide system while some higher Tl-content phases were obtained in the arsenide and antimonide systems. The arsenide system produced a Tl-As phase with an approximate ratio of 7:2, but only in the presence of excess elemental Tl and in an InAs matrix. Under some growth conditions, a ternary InTlAs phase was formed but only in the presence of both InAs and elemental Tl. The antimonide system produced a Tl-Sb phase with a ratio of 7:2 but only in the presence of excess Sb. A ternary InTlSb phase could not be produced, rather a combination of the Tl_7Sb_2 phase and InSb was created.

These phases were characterized by x-ray diffraction, electron microprobe, scanning electron microscopy, secondary ion mass spectrometry and Auger electron spectroscopy. The Tl sticking coefficient was found to depend heavily on the substrate growth temperature. For substrate growth temperature above 425°C the sticking coefficient of Tl is essentially zero. Both pure Tl and all the Tl-containing phases produced by

GSMBE were found to oxidize readily in air. Precautions were taken to minimize exposure of these Tl-containing phases to air so that the characterizational results would remain unambiguous.

A model for the incorporation characteristics of Tl in III-V materials was proposed to explain segregation effects. This model is based on the tendency for cationic behavior in Tl. It is believed that this behavior reduces the tendency for higher molecular weight elements to hybridize the outer most s electrons. Hence, higher molecular weight elements such as Tl cannot attain the sp^3 bonding configuration needed for tetrahedral covalent bonding.

The novel dopant source triisopropylindium-diisopropyltellurium was studied as an n-type dopant in InP. Triisopropylindium-diisopropyltellurium was found to decompose at the low growth temperatures dictated by the sticking coefficient of Tl ($<425^\circ\text{C}$). Record n-type doping concentrations up to $1.4 \times 10^{20} \text{ cm}^{-3}$ with good electrical activation and specular morphologies were obtained in InP. The Te activation was found to be thermally stable up to a temperature of 675°C and dopant diffusion was not observed for anneals as high as 850°C for 1 minute.

The intramolecularly saturated Mg compound, bis-3-dimethylamino-propylmagnesium, was found to form Mg clusters making it unsuitable as a p-type dopant in III-V materials. However, carbon tetrabromide was found to produce record p-type doping concentrations in InSb. Acceptor concentrations as high as $5.6 \times 10^{20} \text{ cm}^{-3}$ were produced. A model for the behavior of carbon in III-V semiconductors was formed based on the relative bond strength of C-III and C-V bonds. The behavior of carbon was found to be linked to a thermodynamic driving force. As the $E_{\text{III-C}} - E_{\text{V-C}}$ strength increases, the tendency for carbon to sit on a group V site increases thereby making carbon behave as an acceptor. The Tl-C bond is relatively weak, thus using this model, carbon is predicted to behave as a donor for TIP, TIAs, TISb and all compositions of InTIP and InTIAs. However, carbon is expected to be an acceptor in InTISb for low concentrations of Tl.

CHAPTER 1 INTRODUCTION

1.1 Motivation and Objectives

Recently there has been a considerable amount of effort in the fabrication of long wavelength infra-red (LWIR) 8 - 12 μ m detectors and focal plane arrays (FPA). Currently, the dominant material for LWIR detectors is mercury cadmium telluride (HgCdTe)^{1,2}. An enormous effort has brought these technologies to a point where arrays as large as 512 x 512 pixels can be manufactured with practical yields and at high, but still acceptable cost. However, the HgCdTe system suffers from a number of fundamental problems that make the use of this material system questionable for more sophisticated devices such as FPA and infra-red emitters. For example, the ability to make larger FPA's has been hampered due to the inability of HgCdTe to be synthesized with a uniform composition over the large detector areas needed³. The HgCdTe bandgap is very sensitive to even slight changes in composition, and, thus, fabrication of larger arrays with uniform device characteristics is difficult. Further complications in the HgCdTe system become apparent during processing and integration. HgCdTe must be bump-bonded to the substrate electronics⁴. In most cases the read out integrated circuits are based on silicon. This creates difficulties in the thermal stability of the array, such as its operation at elevated temperatures and the physical size of the array that can be fabricated⁵.

The ability to form an infra-red emitter is also seriously in question in the HgCdTe system. With a 17% mismatch with CdTe substrates, a large number of defects occur in the HgCdTe layers that severely degrade the device performance. These defects can act as

trapping centers and cause current leakage of the respective device. As future demands are made for still higher signal-to-noise at higher operating temperatures, multi-spectral response, larger arrays of smaller pixels, longer operational lifetimes, and lower production costs, it is unlikely that the HgCdTe material system will be able to meet these demands.

Because of the maturity and considerable progress in III-V materials in the past two decades, several other device schemes or material systems have been recently investigated or suggested to meet the aforementioned criterion. These can roughly be broken up into three groups. First is the use of strained layer superlattices in existing III-V technology^{3,6,7}. An example of this material system is AlGaAs/InAs. Second is the replacement of a normal group V element such as As with a larger group V element such as bismuth (Bi)⁸⁻¹⁴. Examples of these include, Bismuth in InAs, InSb, or InAsSb. The last method is the replacement of a group III element with a larger group III such as thallium (Tl)¹⁵⁻¹⁹. Examples here include Tl in InP, InAs and InSb.

The method of replacing the matrix group III element with a larger one such as Tl will be the focus of this dissertation. Recently, $\text{In}_{1-x}\text{Tl}_x\text{P}$ ¹⁶, $\text{In}_{1-x}\text{Tl}_x\text{As}$ ¹⁶ and $\text{In}_{1-x}\text{Tl}_x\text{Sb}$ ¹⁵ have been proposed as potential candidates for LWIR applications. They are predicted to have the high carrier mobilities and infrared absorption needed for high performance devices. $\text{In}_{1-x}\text{Tl}_x\text{P}$, $\text{In}_{1-x}\text{Tl}_x\text{As}$ and $\text{In}_{1-x}\text{Tl}_x\text{Sb}$ are predicted to have a lattice parameter less than 1.5-2% larger than that of InP, InAs and InSb, respectively, for alloy compositions of $x=1$. In addition to the favorable lattice parameter, a desirable band gap of 0.1 eV is predicted at a composition of $x=0.67$ for $\text{In}_{1-x}\text{Tl}_x\text{P}$, $x=0.15$ for $\text{In}_{1-x}\text{Tl}_x\text{As}$, and $x=0.09$ for $\text{In}_{1-x}\text{Tl}_x\text{Sb}$. All of these alloys are expected to cover the entire IR range due to the negative bandgaps of the semi-metal binary compounds TIP, TlAs, and TlSb^{15,16}.

To this point the Tl-containing alloys have only been predicted theoretically. Thus, it is evident that experimental work is needed to examine the practicality of these theories and the feasibility of fabricating and properly doping device quality material. With this in mind, the work presented here has five principal objectives: first, to test the theory

presented by M. van Schilfgaarde et al. and provide experimental feedback to help improve their model; second, to identify experimentally the growth regimes needed for the synthesis of Tl-containing alloys, and determine the maximum incorporation of Tl in each of the respective matrices; third, to determine the crystal structure of the binary Tl-containing and ternary InTl-containing alloys; fourth, to correlate the composition of the TlV and InTlV alloys with its band properties and structure, and finally, to evaluate suitable n- and p-type dopants for the Tl-containing materials accounting for any specialized growth parameters needed.

1.2 Background Information

Relevant material on both the theory and the growth of the Tl-containing alloys will be discussed. Included with the theory will be a brief explanation of how the TlV and InTlV material parameters were calculated. A basic review of common III-V n- and p-type dopants will be presented. The ability of the dopants presented to provide suitable dopant characteristics will be discussed, keeping in mind the specialized growth conditions necessary for the Tl compounds.

1.2.1 Theoretical Predictions and Calculations

On the basis of a first principles calculation using the density functional theory, M. van Schilfgaarde et al. argued that $\text{In}_{1-x}\text{Tl}_x\text{P}$ could be formed as a rugged semiconductor material in a zincblende crystal structure throughout all compositions x . Included with this prediction was that $\text{In}_{1-x}\text{Tl}_x\text{P}$ was to have a lattice constant nearly matching that of InP. InTlAs was also proposed to be a viable material for long-wavelength infra-red (LWIR) applications, but it would be closest lattice matched to InAs which is a less suitable substrate than InP. Assuming that these materials could be fabricated in a zincblende

structure throughout the entire compositional range, some of their key structural properties were calculated by the local density functional (LDF) theory. The mechanical and structural properties that the LDF predicts are in good agreement with experimental results for all other known zincblende semiconductors²⁰. In a subsequent paper InTlSb was introduced as having the same potential for LWIR applications as InTlAs and InTlP but, was only predicted to occur in a zincblende structure for Tl concentrations $\leq 10\%$ ^{15,16}.

Further calculations were derived from the linear muffin tin orbital (LTMO) method. Table 1 shows some select material properties of Tl- containing binary and InTl- containing ternary alloys. The values shown in Table 1 have slight corrections to the local density approximation (LDA) theory. Errors in the LDA are small but systematic, thus corrections based on other zincblende semiconductors, specifically the errors in the overbinding of zincblende semiconductors can be accounted for and removed²¹.

As shown in Table 1.1, the lattice parameters as predicted by the LDA are 1.5 - 2% larger for TIP, TlAs and TlSb than there respective substrates InP, InAs and InSb, respectively. LDA also predicts negative bandgaps for TIP, TlAs and TlSb. This indicates that alloys of these Tl-containing materials with In should be able to span the entire infra-red (IR) region.

By mapping the LDA bands with a tight binding Hamiltonian, van Schilfgaarde et al. examined the band structures of TIP and TlAs. From this method including some corrections from the coherent potential approximation, the compositional dependence of these alloys are shown in Figure 1.1. This approximation approach has been extensively tested in zincblende semiconductors and has been found to be quite accurate, with errors typically < 0.1 eV²².

Table 1.1: Select properties of the Tl-containing alloys^{15,16}. (E_b - cohesive energy, B-bulk modulus, % mismatch is to respective group V substrate.)

Property	TlP	TlAs	TlSb	In _{0.33} Tl _{0.67} P	In _{0.85} Tl _{0.15} As	In _{0.91} Tl _{0.09} Sb
E_b (eV)	-0.27	-1.34	-1.60	0.1	0.1	0.1
E_h (eV/atom)	3.26	3.11	2.86	3.43	3.52	-
a_0 (angstroms)	5.96	6.18	6.59	5.93	6.08	-
% mismatch	1.53	1.98	1.70	1.02	0.33	-
B (10^{12} erg/cm ³)	0.57	0.49	0.38	0.61	0.58	-
μ_c @ 80 K (10^5 cm ² /V*s)				60.0	1.16	-
μ_e @ 200 K (10^5 cm ² /V*s)				4.50	6.72	-
Crystal Structure	ZB	ZB	CsCl	ZB	ZB	x<.2 ZB x>.2 CsCl

In Figure 1.2, the predicted structural stability of the Tl containing compounds is shown relative to the more common III-V materials. These properties were calculated by M. van Schilfgaarde et al. using the LDA theory with some minor corrections to compensate for error in the predicted ground state energies of free atoms^{20,23,24}. This helps determine the structural stability of the Tl-bearing compounds to other known zincblende semiconductors. Thus, by comparing the binding energies of the zincblende (ZB), sodium chloride (NaCl) and the cesium chloride (CsCl) structures for the nine In, Ga and Al cations with the anions P, As and Sb, a comparison can be made to the three Tl-

bearing binary structures. Generally, the lighter and more strongly bound III-V compounds favor the zincblende structure, while the heavier and weaker bound materials tend to favor the close-packed structures. As the binding becomes weak, the energy difference between the open and close-packed structures decreases and weakens the two-center bond. Thus for the heavier elements, the ratio of the energy gained by formation of a bond divided by the energy cost needed to form an sp^3 bonding configuration decreases making it more likely to form a close-packed structure. Although TlSb is predicted to favor the CsCl structure, for small atomic percentages of Tl ($x < 0.2$) in $In_{1-x}Tl_xSb$, the zincblende structure is expected to dominate. This is in contrast to the $In_{1-x}Tl_xP$ and $In_{1-x}Tl_xAs$ systems where the zincblende structure is expected to dominate throughout the entire compositional range¹⁶.

1.2.2 Previous Experimental Work on Tl Containing Materials

Prior to this research, only two reports of thallium containing III-V materials were available. The first was from C.E.C. Wood et al., who attempted thallium incorporation into InSb by molecular beam epitaxy²⁵. Using the initial theory by Y. Kanai et al.², Wood attempted to dilate the InSb lattice with a larger group III element, such as Tl, or a larger group V element, Bi. Wood et al. found that the addition of Bi to InSb resulted in the production of a solid solution of Bi and Sb occurring in a second phase solid solution. The same authors also studied the incorporation of Tl in InSb by secondary ion mass spectroscopy (SIMS) for different Tl fluxes and substrate temperatures. It was found that at temperatures above 300°C desorption of Tl from the surface competed with Tl incorporation. At temperatures below 300°C, it was found that Tl incorporation increased as did the accumulation of Tl at the surface. Wood believed the behavior of Tl with changing surface stoichiometry indicated that the Tl was incorporating in a manner consistent with Tl sitting on an In lattice site.

None of the data presented in Wood et al. quantified the amount of Tl that was being incorporated due to a lack of accurate Tl standards. An estimation was made by taking a ratio of the reduction in the In^+ and Sb^+ ion intensities. He estimated the near surface concentration of Tl to be approximately 5 atomic percent. This high surface concentration of Tl persisted even with the highest Sb_4 fluxes. Wood believed that this was enhanced by the formation of a liquid Tl-Sb surface phase. Finally, Wood stated that all films doped with Tl showed little if any wavelength change in the absorption edge and x-ray lattice parameter measurements showed no significant lattice dilation due to Tl incorporation.

The second group with experimental work in the Tl-containing materials was Y. H. Choi et al. at Northwestern University^{18,26}. These papers also focused on the incorporation of Tl in InSb, but the growth technique in this case was low pressure metalorganic chemical vapor deposition (LP-CVD). In the first paper, Choi et al. report the growth of some unknown composition of $\text{In}_{1-x}\text{Tl}_x\text{Sb}$. Choi substantiates his findings with 1) Nomarski optical micrographs of the surface which though not shown are reported to be specular; 2) four crystal x-ray rocking curve measurements that show a shift in the x-ray peak of ~ 3600 arc-sec to the compressive side of the InSb (004) peak; 3) absorption measurements that suggest a decrease in the band gap to approximately $8.5\mu\text{m}$; and 4) a slight enhancement of the low temperature Hall mobility of the Tl-containing InSb film.

In the second paper, Choi et al. report the formation of more InTlSb layers though of unknown composition. This claim is substantiated by three techniques. First, Auger electron spectroscopy (AES) surface scans were presented, though no depth profiling for any of the samples were shown. Second, photoconductive response was shown at both 77 and 300K. The 300K signal was very noisy with no apparent shift, while at 77K the InTlSb sample showed a shift in the absorption edge from $\sim 5.5 - 8.0\mu\text{m}$ wavelength. This shift is not a sharp absorption edge as is the case for the InSb sample grown without Tl but nevertheless, a band gap decrease of 70 meV was reported. This shift in turn was used to

estimate a Tl concentration of 4% assuming Vegard's law and using the SRI predictions for TlSb. Finally, optical transmission of these InTlSb layers is presented. This shows higher overall absorption for the Tl containing sample and an absorption tail extending up to 8 μ m, although once again the shift in the band edge is very gradual.

One further paper could be found in the literature at from P.T. Staveteig et al. a colleague of Choi at Northwestern²⁷. This paper focuses on electrical characteristics of the previously grown In_{1-x}Tl_xSb. Staveteig reports here that the photoresponse of the material extends to 8 μ m at 77K. Also, the absolute magnitude of the photoresponse was measured as a function of bias. The specific detectivity was estimated to be $3 \times 10^8 \text{ Hz}^{1/2}\text{cmW}^{-1}$ at 7 μ m wavelength.

1.2.3 Summary

It is evident that there is a substantial body of theoretical work supporting the possibility of incorporating Tl into III-V materials such as InP, InAs and InSb for IR applications. From the calculations by M. van Schilfgaarde et al., it is believed that the binary Tl containing alloys TIP, TIAs, and TlSb will have negative bandgaps. If these semi-metals can be formed epitaxially, the capability of fabricating vertical devices becomes a possibility, as these semi-metals can be used to form epitaxial ohmic contacts. Unlike metal contacts, epitaxial ohmics offer the unique possibility of epitaxial growth on top of the contacts. This would make possible vertical, as well as horizontal, device fabrication and integration²⁸.

The ternary compounds are believed to be of significant value also. Having a smaller mismatch to commercial substrates than the current standard technology, HgCdTe, should enable cheaper and better performing IR devices such as IR detectors, emitters and FPA's. The formation of these materials should also afford the opportunities for the integration of photonic and electronic devices on the same substrate. This would reduce the

necessity of bump-bonding to Si, improve the high temperature operation and eliminate limitations that exist in the current HgCdTe technology.

All of the initial experimental work in the Tl containing III-V systems for IR applications has been in the InTlSb material system. Wood et al found that Tl has problems with surface segregation similar to that observed during incorporation of Sn in III-V materials. Wood also infers the formation of InTlSb with a Tl concentration estimated by SIMS to be near 5%. However, he does not rule out the possibility that his results could be due to the formation of an Sb and Tl containing phase near the surface of his samples. Finally, Wood reports that he had no significant increase in the lattice parameter of the InSb layer and that these samples showed no significant shift in the absorption edge.

Choi and Staveteig also claim to have fabricated InTlSb with an approximate composition of 5% Tl. The only structural analysis of these films was performed with high resolution x-ray, in which the x-ray peak shifts towards the biaxial tensile side. This is opposite to that predicted by SRI. Due to the lack of research in the Tl-containing materials, the Tl-In and Tl-Sb bond lengths are not known so that it is not possible to conclusively state which direction the lattice should shift. However, the overwhelming trend in other III-V materials when a larger group III element is added to a smaller lattice is a shift towards biaxial compression and uniaxial tension. Auger surface scans were presented showing Tl at the surface of these layers. Due to Wood's initial work suggesting a problem with surface segregation, it is likely that segregation is occurring here as well though depth profiles are needed for more conclusive proof. All other substantiation of InTlSb formation was optical or electrical. These results showed minimal shifts in the band edge towards the 8-12 μ m wavelength regime.

No optical or scanning electron microscopy (SEM) of Tl containing films could be found. Only Two phases of Tl and P, As, or Sb could be found in the JCPDS files. These are Tl_7Sb_2 ²⁹ and TlSb_{15} ³⁰. Finally, no mention of the stability of Tl containing

compounds could be found either in theoretical or experimental data in press, though Tl itself is known to oxidize rapidly in air³¹.

1.3 Scope of the Present Work

The work presented here will be divided into eight chapters. Chapter 2 will detail growth mechanisms in gas-source molecular beam epitaxy (GSMBE). The experimental details of fabricating the Tl-containing alloys will be discussed as well as the methods used to supply reactants to the growth surface for the group III, group V and dopant sources. Furthermore, an explanation of the characterization techniques will be presented as well as the procedures used for the transport and storage of the Tl-containing materials.

Chapter 3 will contain the results of the Tl - P system. Both the binary TIP and the ternary InTIP results will be presented. These results will be compared with recent results found in the literature.

Chapter 4 will present the results of the Tl - As system. Both the binary Tl-As and ternary In-Tl-As results will be presented. These results will be compared to the phosphide system and their overall feasibility will be examined.

Chapter 5 will contain the results of the Tl - Sb system. Both the binary Tl-Sb and the ternary In-Tl-Sb results will be presented. The impact of these results will be discussed with what has recently been published in these material systems. The technical relevance of these materials will also be examined.

Chapter 6 will focus on n-type dopants suitable for use with the specialized growth conditions of the Tl-containing materials. Specifically, the dopant source Triisopropylindium-diisopropyltellurium will be evaluated and doping characteristics will be discussed.

Chapter 7 will focus on p-type dopants suitable for use with the growth conditions mandated by the Tl-containing materials. Carbon-tetrabromide and bis-3-dimethylamino-

propylmagnesium are the p-type dopant sources that will be evaluated. In addition, a model for the behavior of carbon in III-V materials will be presented.

Finally, in Chapter 8, important conclusions are stated along with recommendations for future research in Tl-containing materials.

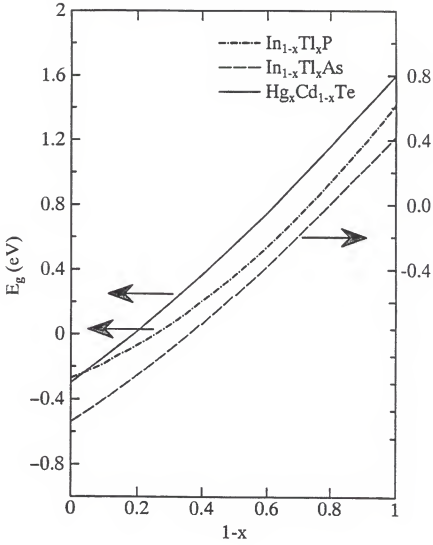


Figure 1.1: Bandgaps of $\text{In}_{1-x}\text{Tl}_x\text{P}$, $\text{In}_{1-x}\text{Tl}_x\text{As}$, and $\text{Hg}_x\text{Cd}_{1-x}\text{Te}$ over the entire compositional range as predicted by mapping the LDA bands.

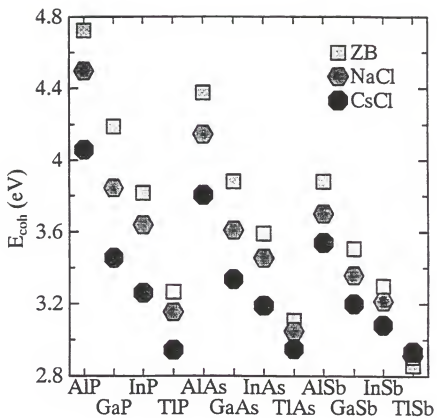


Figure 1.2: Cohesive energies of select III-V compounds in the zincblende, NaCl, and CsCl structures.

CHAPTER 2 EXPERIMENTAL

2.1 Description of the Growth Process

The majority of the samples studied in this dissertation were grown by gas-source molecular beam epitaxy (GSMBE) using a Varian Gas Source Gen II. Specific explanations of the growth conditions used will be presented in later sections of this dissertation. Furthermore, a comprehensive review of the sources and dopants available for the growth of the Tl-containing will be discussed.

2.1.1 Gas Source Molecular Beam Epitaxy

Gas-source molecular beam epitaxy (GSMBE) has become a powerful growth technique that has been instrumental in the fabrication of new electronic and photonic materials³². GSMBE is a hybrid growth technique that utilizes key components of both molecular beam epitaxy (MBE) and metal organic chemical vapor deposition (MOCVD). Growth using GSMBE allows one to combine some of the more desirable characteristics of MBE and MOCVD. Some of these characteristics are (i) ability to grow uniform ultrathin layers in a controllable and reproducible fashion; (ii) excellent control over thickness, selectivity and compositions; (iii) ability for in-situ characterization such as reflected high energy electron diffraction (RHEED); (iv) elimination of need for group V source replenishment; and (v) increased scale-up potential. A comparison of the features of GSMBE compared to that found in metal organic molecular beam epitaxy (MOMBE), low

pressure metal organic chemical vapor deposition (LPMOCVD), MBE and MOCVD are shown in Table 2.1³³.

Table 2.1: Relationship between various epitaxial growth techniques.

<u>Technique</u>	<u>Sources</u>	<u>Pressure (torr)</u>	<u>Flow Regime</u>
MOCVD	Gas	760	Viscous
LPMOCVD	Gas	$100\text{-}10^{-2}$	Viscous
MOMBE	Gas	$\leq 10^{-4}$	Molecular
GSMBE	Solid III, Gas V	$\leq 10^{-5}$	Molecular
MBE	Solid	$\leq 10^{-9}$	Molecular

Because of the variation in growth pressure regimes and precursor species, the kinetics of growth for each deposition technique vary. Deposition in an MBE environment occurs in a high vacuum such that the sources that arrive at the heated substrate have a longer mean free path than the distance from the source to the substrate. Thus, molecules beams do not collide before arrival at the growth surface. At pressures above 10^{-3} torr, the molecular flow regime gives way to viscous flow. In viscous flow, the molecular beams no longer have the ability to travel the entire source to substrate distance without collisions.

The chemistry of GSMBE is only slightly more complex than MBE. Elemental sources supply atomic beams in the same fashion as MBE. In MBE, the group III atomic beams impinge on a heated substrate surface, migrate to the appropriate lattice sites, and deposit epitaxially in the presence of excess group V species. The growth rate is determined by the arrival rate of the group III atomic beams and the sticking coefficient of the group III species on the heated substrate at a given temperature. Since the group III

atoms are generated by thermal evaporation of solid elemental sources, there are no chemical reactions involved for source extraction like that of MOCVD or MOMBE.

Differences between MBE and GSMBE arise in the supply of the group V species. Instead of using elemental sources as in MBE, GSMBE uses a gaseous precursor such as phosphine (PH_3) for the group V species necessary for growth of these materials. Often these gaseous sources will need assistance to decompose into a monatomic or diatomic group V beam. The kinetics of this will be discussed in detail later in this chapter in the section on group V sources.

MOMBE is progressively more complex than GSMBE. In MOMBE, both the group III and group V sources are gaseous. Deposited in the molecular flow regime, the group III molecules do not react until desorption on the growth surface. The chemistry in MOMBE is more complex than in MBE, but the situation is simpler than in MOCVD where the presence of a boundary layer and the simultaneous involvement of gas- and adsorbed-phase reactions introduces additional complexities. In atmospheric MOCVD, the group III alkyls, typically carried in a gas stream of H_2 , often undergo partial dissociation. They then diffuse through a stagnant boundary layer above a heated substrate and further dissociate into atomic group III elements as illustrated in Figure 2.1. The group III adatoms migrate to the appropriate lattice sites and deposit epitaxially by combining with a group V atom on the heated substrate surface. The growth rate is found to be limited by the diffusion rate of the group III alkyls through the boundary layer at normal growth temperatures, and at low temperatures it is limited kinetically by the rate of pyrolysis of the precursors as shown in Figure 2.2. The growth mechanisms in MOCVD, however, make it difficult to grow abrupt doped layers and to accurately deposit very thin films. In MOCVD, gas-phase (parasitic) reactions between some selected reactants can also occur and while beneficial to aid in the removal of unwanted impurities, can lead to poor incorporation efficiency and non-uniform growth.

The major difference between MOMBE and GSMBE is that in GSMBE, group III sources are elemental while in MOMBE group III sources are gaseous. The growth chamber for these systems are normally similar having the majority of the same components. Usually the MOMBE system will have a larger pumping capacity to counteract the larger volume of gas that the gaseous sources create. Both the MOMBE and GSMBE chambers are similar to that of a standard MBE chamber. A typical MOMBE/GSMBE chamber is shown in Figure 2.3. Upon examination of the chambers, the main difference is that one or more of the effusion cells have been removed and replaced with a group III or group V injector. Generally in GSMBE dopants are supplied by elemental effusion ovens although some systems are now beginning to incorporate gaseous dopant sources.

In the case of MOMBE, the metal-organic sources are stored in stainless steel bubblers. These bubblers can vary both the temperature and pressure of the source. A carrier gas such as H or He is used to extract the reagent from the bubbler and transport it to the growth chamber. The amount of flow to the chamber is regulated by a mass flow controller, and this in conjunction with the pressure and temperature variations available in the bubbler, make it possible to control the amount of group III source that reaches the substrate. In MOMBE the metal-organics do not undergo decomposition until they interact with the heated substrate. An injector temperature of 65°C is used to prevent the metal organics from condensing in the injector. The choices of group III sources that are to be used in the growth of the novel TI-containing compounds will be discussed later in this chapter^{32,33}.

The vast majority of samples were In-mounted to a backing wafer of Si. Often this changes the growth temperature of the In-mounted material. Due to low growth temperatures, the use of a pyrometer was deemed too inaccurate. Instead, the temperature was measured by a substrate thermocouple and calibrated by mounting pieces of InSb to the Si wafer and slowly increasing the temperature until the InSb began to melt. Knowing

the melting temperature of InSb to be 525°C and correlating this with the temperature indicated by the substrate thermocouple allowed for a more precise method for determining the temperature. This method found the substrate thermocouple to be accurate to $\pm 10^\circ\text{C}$.

2.2 Mechanisms of Epitaxial Growth

Epitaxy refers to the arrangement of atoms upon a single crystal surface or wafer such that the lattice structure of the epilayer is determined by that surface. In order for epitaxial growth to occur there must be a "template" for the adatoms to utilize that is continuous across the entire wafer surface. When the deposited material is the same as the substrate, the epitaxial phenomena is called homoepitaxy. If the material differs from that of the substrate, it is referred to as heteroepitaxy. An example of homoepitaxy is InP on InP, while an example of heteroepitaxy is GaAs on Si.

Heteroepitaxial growth can be either lattice matched or lattice mismatched. In lattice matched systems, the bulk lattice constant of the epitaxial layer is identical to the lattice constant of the substrate. Examples of this include $\text{Al}_{0.5}\text{In}_{0.5}\text{P}/\text{GaAs}$. In lattice mismatched systems, the lattice constant of the epitaxial layer is different from that of the substrate. For such a system, where a_e = bulk lattice constant of the epilayer material and a_s = lattice constant of the substrate, the mismatch can be described by

$$f = \frac{(a_s - a_e)}{a_s}$$

The growth of lattice mismatched material can lead to a variety of strain relieving mechanisms such as dislocation formation, change in growth mode, and film cracking, all of which may degrade the quality of the epilayer. There are numerous factors that impact the quality of the epilayer that occur either at the initial stages of growth or during the

deposition of the film. Growth temperature, source impurities, substrate orientation and surface cleanliness can all influence quality of the epilayer. Other factors such as the relationship between surface kinetics and growth parameters allow the creation of metastable configurations in a film. Examples of these parameters include deposition rates and substrate temperature.

Epitaxial growth is realized on a substrate surface and proceeds through a sequence of steps as illustrated in Figure 2.4 where the more important processes are as follows:³⁴

- 1) adsorption of the impinging molecules or constituent atoms on the substrate,
- 2) dissociation and surface migration of the adsorbed molecules,
- 3) incorporation into the crystal lattice of the substrate or the epilayer,
- 4) thermal desorption of the species that were not incorporated into the lattice.

The deposition of an epitaxial film is a fairly complex process. Impinging beams of either atoms or molecules onto a heated substrate can lead to adsorption of the precursor species. For epitaxy to occur, molecular precursors must first undergo a decomposition process yielding an adsorbed atomic species on the substrate surface. Adatoms can migrate along the surface by jumping over activation energy barriers E_D at saddle points between neighboring adsorption sites. The adatoms may reevaporate after a mean stay time t_s , depending on the substrate temperature T_s and the activation energy E_a , or migrate a distance λ_s .³³

There are preferred sites for adsorption on the substrate surface. Deposited atoms on the surface seek atomic sites that minimize the total energy of the system. An isolated atom on a surface adds dangling or unsatisfied bonds to the system and raises the total energy. The number of free bonds can be reduced by adsorption at surface defects such as steps, kinks, and screw dislocations. In addition, islands themselves can be thought of as surface defects providing high-energy binding sites for further atom attachment during deposition^{35,36}.

The growth of these epilayers develops according to one of three distinct thermodynamically derived growth modes as illustrated in Figure 2.5: layer-by-layer (Frank-van der Merwe or 2D); nucleation of three-dimensional islands on a bare substrate (Volmer-Weber or 3D); and formation of three-dimensional islands on a microscopically thin uniform layer (Stranski-Krastanov). The ideal mechanism of growth of device films is by layer-by-layer deposition of the film atoms. Films grown in this fashion are planar and the thicknesses of the films are more easily controlled. Many materials, however, do not deposit on the substrate in the layer-by-layer mode and it is in fact more common to observe deposition occurring by the formation of islands at the very early stages of growth followed by their coalescence resulting in a continuous film having a rough surface morphology³⁷⁻³⁹.

Thin film growth is a very complex process that requires control of many variables for the deposited film to be relatively free of defects and to have good surface morphology. As devices become more sophisticated and device regions become smaller, the ability to control defect formation becomes even more important. Understanding the kinetics of growth, the types of growth and the variables that affect these parameters is essential. These reactions at the surface and how certain types of elements or precursors will incorporate is fundamental for attempting the growth of new electronic materials such as the Tl-containing alloys.

2.3 Dopant Sources

2.3.1 Growth and Characterization of Te-doped InP

The epitaxial layers in these InP samples were grown by MOMBE in an INTEVAC Gas Source Gen. II on 2 inch diameter Fe doped, (100) InP substrates. Substrate growth temperatures ranged from 375 - 525°C as measured by a substrate thermocouple.

Triethylindium at a bubbler temperature of 13.2°C was used as the In precursor and was transported by a H₂ carrier gas with a flow rate of 15 sccm and a pressure of 6 Torr. Under these conditions a growth rate of ~100Å/min. was obtained. Phosphine (PH₃) was used as the phosphorous source after decomposition in a low pressure cracker maintained at 1000°C. Phosphine flows ranged from 1 to 20 sccm. The majority of the samples were grown with 1 sccm of phosphine while the higher flows were necessary for the high V/III ratio experiments. TIPIn-DIPTe was employed as the Te source and was maintained at a bubbler temperature of -9.1°C while the bubbler pressure ranged from 6 to 95 Torr and a H₂ carrier flow gas rate of 0.5 to 10 sccm. The low temperature was necessary to achieve the appropriate doping concentrations due to the high incorporation efficiency of the source.

Hall data was collected using the van der Pauw method utilizing RTA-alloyed In contacts ($T_a=380^\circ\text{C}$). Epilayer lattice dimensions were deduced from symmetric (ω -2 θ) x-ray rocking curves obtained with a Phillips, high-resolution five-crystal diffractometer. Micro-graphs of the samples surface morphologies were provided by using a JEOL 6400 scanning electron microscope (SEM). Secondary ion mass spectroscopy (SIMS) profiles were obtained from Evans East using a Cs⁺ beam in a PHI 6300. Samples for annealing were doped to an electron concentration of $1.4 \times 10^{20} \text{ cm}^{-3}$.

2.3.2 Growth and Characterization of C-doped InSb

InSb layers were grown in a Varian Gas Source Gen II on (100) InP:Fe substrates which were In-mounted to Si backing wafers. Elemental In and Sb were used as the Group III and Group V sources, respectively. Substrate temperatures ranged from 325 to 450°C as measured by the substrate thermocouple. CBr₄, maintained at a temperature of 0.1°C, was used as the dopant source, and was transported with a He carrier gas. Bubbler pressures and carrier gas flow rates were varied from 35 to 99 Torr and 0.5 to 20 sccm.

Hall measurements were performed using the Van der Pauw method. Lattice constants were obtained from symmetric ($W/2q$) x-ray rocking curves from a Phillips, high-resolution five-crystal diffractometer. Secondary ion mass spectroscopy profiles were obtained from Evans East using a Cs^+ beam in a PHI 6300.

2.4 Source Chemistry

The use of ultra-high vacuum (UHV) growth techniques such as gas source molecular beam epitaxy (GSMBE) for the deposition of semiconductors offers a number of advantages. The absence of gas phase interactions allow for precise control of thickness, uniformity, and composition using a variety of gaseous and elemental sources. The sources used in the attempts to grow Tl-containing III-V alloys are described below.

2.4.1 Group III Sources

Elemental thallium (Tl) was the primary Tl source employed for the growth of Tl-V and InTl-V materials. The elemental Tl was resistively heated in an effusion oven to provide a sufficient flux. When Tl is resistively heated, monovalent Tl is the majority species evolved from the effusion oven. It is expected that the monovalent Tl state will create difficulties enhancing segregation of Tl in III-V compounds. It is hoped that the growth parameters can be altered sufficiently to overcome these problems.

There is only a limited volume of information regarding the use of gaseous Tl precursors. Cyclopentadienyl-thallium (CpTl) has been reported for deposition of InTlSb by MOCVD^{26,27}. The low vapor pressure of this compound, shown in Figure 2.6, mandates the use of relatively high, $\sim 50\text{-}60^\circ\text{C}$, bubbler temperatures⁴⁰. Such temperatures most likely produce severe decomposition of the source in the bubbler or the transport lines. While the low pressures in GSMBE and MOMBE may allow this temperature to be

reduced somewhat, the ability to transport this source efficiently remains a concern. In addition, it should be noted that the Tl delivered to the growth surface by CpTl, like that produced by resistively heating elemental Tl, is monovalent, while the desired state of Tl for InTIP is trivalent. In order for the Tl produced by the decomposition of CpTl to react with phosphorous, the s and p orbitals must be hybridized at the growth surface. Energy calculations suggest that the energy required to accomplish this transformation is 2-3 times higher than that of other Group III atoms^{31,41}.

Both elemental Tl and CpTl are water soluble compounds. This makes absorption of Tl through the skin possible and the chance of Tl poisoning a strong concern. Consequently, precautions must be taken when using CpTl in systems which are difficult to purge, such as the stainless steel chamber found in GSMBE and MOMBE. Finally, elemental Tl oxidizes rapidly in the presence of air. Further precautions during storage and characterization may be needed if the Tl-containing materials are found not to be stable in air.

Both elemental indium and triethylindium (TEIn) were used as In sources for the Tl-containing compounds. Elemental In can be used for low (~200°C) substrate growth temperatures without the risk of incomplete decomposition that would occur with the use of gaseous In precursor molecules. The growth of In containing compounds from elemental In by GSMBE is usually performed at substrate temperatures below 540°C in order to prevent desorption of In from the growth surface. The dependence of In and Tl vapor pressure on temperature is shown in Figure 2.7⁴². This figure suggests that the incorporation of Tl at the growth surface above ~425°C may be limited due to a high rate of desorption. As a result low growth temperatures will most likely be required to deposit significant amounts of Tl to the growth surface.

Increased desorption from the growth surface is in fact what we see as the vapor pressure curve in Figure 2.7 predicts^{42,43}. Figure 2.8 shows samples grown under the same exact cell temperature but at three different substrate temperatures. The SEM images

clearly shows a decreased Tl droplet density for samples grown at elevated temperatures. Desorption of Tl from the growth surface becomes noticeable at 325°C and the sticking coefficient approaches zero at temperatures above 425°C. This is consistent with the results of Wood et al²⁵.

Although trimethylindium (TMIn) is the most commonly used alkyl In source, TEIn was used for the gaseous In source in these experiments because of the aforementioned substrate growth temperature concerns expressed in Figures 2.7 and 2.8. TMIn would not completely decompose at such low growth temperatures allowing unacceptable amounts of carbon to incorporate into the epilayer. Unlike the In-CH₃ bonds in TMIn, the In-C₂H₅ bonds in TEIn pyrolyze at lower substrate growth temperature thus providing a cleaner source of In to the growth surface²⁸. The growth of In-containing materials at temperatures < 475°C has not been extensively studied, although initial experiments have yield no problems with substrate growth temperatures as low as 300°C. Cell temperatures for In and Tl ranged from 860 - 920°C and 490 - 625°C, respectively.

2.4.2 Group V Sources

The source of phosphorous used in these experiments was Phosphine, PH₃. The PH₃ was pre-cracked prior to entering the growth chamber using a molybdenum-catalyzed high temperature cracker maintained at 1000°C^{32,44}. An example of this type of catalytic cracker is illustrated in Figure 2.9. This process evolves subhydrides, monomers, dimers and tetramers. The primary species evolved in this process are believed dimers of P₂ and H₂. Using cracked hydrides as the group V source, the growth of In-containing compounds from elemental In by GSMBE is usually performed below \cong 540°C in order to avoid desorption of In from the growth surface. Phosphine has several advantages over elemental P, such as reproducibility, easier source replenishment, better control of flux and a wider range of V/III ratios possible.

The source of arsenic used in these experiments was arsine, AsH_3 . Much like PH_3 , AsH_3 was cracked at 1000°C prior to entry in the growth chamber. Both gaseous forms of PH_3 and AsH_3 are preferred to solid group V sources because the hydrides can maintain a steady flux over a long period of time and more precise control over the III-V ratio during growth. Although the group V hydrides are generally very dangerous to work with due to their high toxicity, sources can be changed from the growth apparatus without venting the entire growth chamber. Reducing exposure of the chamber to oxygen reduces the risk of ignition of pyrophoric materials in the chamber.

An elemental source of antimony was employed for growth of the antimonides. Elemental Sb was resistively heated in an effusion oven in order to produce a steady source of Sb for maintaining the surface of the growth wafer during oxide desorption and for a steady group V source during growth. The gaseous Sb source stibine, SbH_3 , is available but use of this precursor is limited due to serious problems with the instability of this hydride and the resulting storage problems associated with it. Another gaseous Sb source available is triethylantimony (TESb). This source, however, is expected to be too thermally stable for growth of the TI-containing materials.

2.5 Solubility and Segregation

Upon arrival of the group III and group V species at the growth surface, incorporation of these elements under the proper growth conditions rely on several key factors. Some of these include the choice of sources, thermal energy available at the growth surface, and the ratio of the group III and group V species available for incorporation. All of these have been discussed in the previous sections. Two important factors that have yet to be discussed are possible problems with segregation and solubility.

Segregation is primarily a kinetic problem. Some elements tend to site switch. Hence, one atom tends to ride or float on the growth surface preventing normal

incorporation into the lattice. Segregation effects can be reduced by lowering the substrate growth temperature. By reducing the amount of thermal energy at the growth surface, the energy needed to allow the atoms to site switch is minimized. Hence, the atoms tend to incorporate in a more normal fashion. One consequence of reducing the growth surface temperature is a reduction in surface mobilities of the adatoms. If the adatoms do not have enough energy for proper surface mobility, they may not be able to find the proper lattice locations to form layer by layer epitaxial growth.

Solubility is primarily a thermodynamic problem. If the maximum solubility of one element in a compound is exceeded, a two-phase region will result consisting of the limited solubility element and the compound. Often the solubility can be increased by increasing the growth temperature. However, increasing growth temperature to gain solubility can create problems with segregation as well as changing the sticking coefficient of the individual elements involved in the growth process.

2.6 Safety Issues

In any technical process involving chemicals and/or high voltage systems, safety concerns should always be addressed and procedures adopted before trouble arises. Safety precautions are necessary in the use of highly toxic reactive materials found in GSMBE/MOMBE technology. Most of the MOs are pyrophoric compounds. Fumes resulting from the MO decomposition may cause skin and eye irritation and should not be inhaled. MOs are not a major risk to people provided that sensible precaution is taken in their handling and use. However, group V hydrides such as PH_3 and AsH_3 are very toxic and require that strict safety precautions be used. PH_3 affects the nervous system at a level of 300ppb requiring that it be stored in isolated, exhausted cabinets⁴⁴. The exhaust from the main growth chamber contains many toxic chemical species that are potentially harmful to the environment. Therefore, exhaust is decontaminated in a scrubber system before it is

vented into the atmosphere. To protect the safety of the individuals working with and around the growth system, it is constantly monitored for toxic gas leaks by an MDA detector. If any leaks are detected, an audible/visual alarm will notify the occupants to immediately evacuate the building and all pneumatic valves on the growth system will be automatically switched to the off position to minimize any further escape of the gases.

In addition to these safety issues, respect for systems that employ high voltage or high temperatures must always be taken. Common sense is often not sufficient preparation when dealing with specialized problems that occur in the lab. The author recommends that time for a comprehensive safety review of the chemicals and dangers from the systems themselves be taken before work in the lab begins.

The last safety issue that will be discussed relevant to the work in this dissertation is the handling of Tl. According to the materials safety data sheets (MSDS), Tl is the most toxic nonradioactive metal. Tl is water soluble, therefore it can be absorbed through the skin into the blood stream. Once in the blood stream Tl tends to accumulate in the brain and the testes. Tl poisoning can be identified by whitening around the lips, loss of body hair, and extreme fatigue⁴⁵. Tl is a very dangerous metal and it should be handled with great care. Gloves should always be worn when handling wafers and particulate masks when cleaving Tl-containing wafers. Tl oxidized quickly in air and there are many oxide forms. These oxides have not been studied extensively but common sense would suggest that the same type of care should be given to these materials.

2.7 Characterizational Techniques

Due the ease that Tl metal degrades upon contact with air, a detailed discussion of the handling, storage, transport and characterization of these materials will be presented in this section. This will be followed by a brief description of the characterization techniques

that were used to examine the Tl concentrations, phases created during growth, surface morphologies, crystal structure and lattice parameter.

2.7.1 Sample Handling and Storage

Tl metal oxidizes readily upon exposure to air⁴⁶. Characterization of any oxidized Tl-containing material becomes much more difficult than an oxide free material. Figure 2.10 (a) shows what a typical surface containing Tl looks like after exposure to air for about one day. The accompanying x-ray plot shown in Figure 2.10 (b), illustrates the vastly increased number of x-ray peaks that form upon oxidation. Any addition of such oxide peaks only complicates the identification of the phases present. These Tl-oxides also hamper data collection in both the electron microprobe (EMP) and electron microscopes where charging of the oxide degrades the imaging and masks the phases that are one is attempting to identify.

Following the growth of a Tl-containing sample, the epilayer was kept under vacuum until the characterization process began. Samples were removed from the GSMBE system, cleaved into smaller pieces and placed into a container that could be connected to an inert gas source such as a nitrogen or argon cylinder. A small piece of each sample was attached to SEM mounts while other pieces were mounted in the EMP sample holder. The samples were then sealed in the container, purged with inert gas and transported to the characterization facility. At the characterization facility, the samples were then removed from the sealed container and immediately inserted into the EMP and the SEM respectively. Surface images were first taken to aid in the compositional analysis. Next, the compositional analysis was performed in the EMP. Finally, the samples were removed one by one and x-ray diffraction was initiated. By keeping the sample under vacuum for the longest possible time, unambiguous analysis of the Tl-containing materials could be accomplished.

It was found that long term storage of these materials needed to be carried out under vacuum in order to prevent oxidation. Samples that were not stored in this fashion oxidized quickly and showed no evidence of any TI-containing substance other than TI oxide.

2.7.2 X-ray Diffraction

X-ray diffraction of the TI containing materials was used to provide various types of information about the as grown epilayers. This information included the types of phases present, expansion or contraction of the lattice, and information on the crystal structure of identified phases.

2.7.2.1 Powder x-ray diffraction

X-ray diffraction was employed for the determination of phases and their respective crystal structures using a Phillips APD 3720 x-ray diffractometer. The type of radiation was $\text{Cu}_{K\alpha}$ radiation at 1.54\AA at a bias of 40 kV and a current of 20 miliamps. Scans ranged from an angle of $10 - 90, 2\theta^\circ$ with a 0.5° step at 0.5 second intervals. Very few TI-containing materials can be found in the JCPDS (now known as the ICDD) files⁴⁷. Therefore, it was attempted to take known standards and compare them to unknown samples. This was accomplished by making transparencies of the known growth materials such as substrates and well documented epilayers such as InP and InSb and comparing this data to that found in the TI-containing epilayers. This was done trying to add only one variable at a time such that a clear effect could be determined.

2.7.2.2 High resolution x-ray diffraction

High resolution x-ray diffraction (HRXRD) was used to deduce changes in the epitaxial lattice from the incorporation of TI or the incorporation of either n- or p-type

dopants. HRXRD analysis was conducted using a Phillips 5-crystal x-ray diffractometer. Since HRXRD is somewhat complicated, a brief discussion of the diffractometer set-up, optimization procedures, and the various steps involved in the measurement of lattice strains will be detailed.

The HRXRD system includes an x-ray source, a monochromator, collimator, a goniometer and a detector. The x-ray source is a Cu target anode which is bombarded by accelerated electrons created at a cathode using a generator operating at 40kV. Upon such bombardment, the Cu target emits $\text{Cu}_{K\alpha}$ x-ray radiation at a characteristic wavelength of 1.54\AA . The x-ray beam, thus created, has a broad angular and wavelength range and needs to be monochromatized and collimated prior to its impingement upon the specimen. The monochromator/collimator used in the Phillips system consists of four highly perfect germanium crystals as is shown in Figure 2.11. The crystals are cut in such a way that either their (440) or (220) planes could be used for diffraction. The crystals are aligned so as to reduce spectral dispersion and peak broadening of the incident x-ray beam.

The goniometer sample stage has three independent degrees of freedom for motion in spherical coordinate space. The sample can be rotated about its surface normal (z axis), tilted about the x axis and rocked about the y axis. The angle between the detector and the sample surface is defined as $2\theta - \omega$ where ω is the angle between the fixed x-ray source and the sample surface. The ability to rock the specimen and move the detector independent of the specimen is used in the alignment of the diffractometer.

There are two types of HRXRD rocking curve scans based on the variation of ω and/or 2θ that were used in this work. The ω scan, where the detector is maintained stationary while the specimen rocks over a specified angular range and the $\omega/2\theta$ scan where the range of ω is specified but the specimen is rocked over the specified angular range along with the detector which sweeps over the same range. The result is the angular variation of 2θ being twice that of ω . Such a scan where ω and 2θ can be individually specified is quite different from a $\theta/2\theta$ scan performed using a conventional diffractometer

where only the q value is specified and cannot be used in cases where $\omega \neq q$. The $\omega/2q$ scan is used when the specimen is composed of more than one material and the Bragg conditions of only one of the materials is known.

In order to obtain the true ω values for epilayer and substrate, the rotation angle has to be optimized. Since the Bragg angle of the epilayer is not known, ω scans are initially conducted at a fixed substrate Bragg angle ($2q$ fixed) and a optimal rotation angle for the substrate peak is obtained. An $\omega/2q$ scan is then performed about the substrate peak to determine the Bragg angle of the epilayer. This Bragg condition is used for further scans to optimize the epilayer peak value. In order to obtain accurate values for ω , the rotation needs to be optimized to an accuracy of $< 1^\circ$.

Strain determination in the lattice can be found by examining the peak position ω of the substrate peak in a symmetric plane, such as the (004) plane. This plane is symmetric because the angle of incidence equals the angle of reflection as the sample surface is oriented to the (001) plane, can be used to determine the spacing, d , between the (004) planes from Bragg's law given by

$$n\lambda = 2d \sin \theta$$

where λ is the wavelength of the incident radiation and θ is the Bragg angle given by $\omega = 2\theta$ for a symmetric reflection. The angular separation between substrate and epilayer peaks for the symmetric (004) reflection can be used to determine the perpendicular lattice-mismatch between epilayer and substrate given by

$$\left(\frac{a_{\text{epi}} - a_{\text{sub}}}{a_{\text{sub}}} \right)_{\perp} = -(\theta_{\text{epi}} - \theta_{\text{sub}}) \cot \theta_{\text{sub}}$$

where a is the lattice parameter and the subscripts "epi" and "sub" stand for the epilayer and substrate, respectively.

In general one must distinguish between the mismatch perpendicular and parallel to the epilayer/substrate interface. These mismatch components can be determined by using HRXRD rocking curves from asymmetric lattice planes making an angle ψ with the crystal surface⁴⁸.

2.7.3 Electron Microprobe

A JEOL 733 electron probe x-ray microanalyzer was used to determine the composition of the different phases that occurred in the growth of the Tl-V and InTlV. Microprobe is a nondestructive quantitative and qualitative elemental analysis technique that measures characteristic x-rays emitted from a target. The physical basis of electron probe microanalysis is the generation of characteristic x-rays through the bombardment of a sample with energetic electrons. The x-rays are produced by way of ejection of core level electrons (inelastic scattering) followed by the de-excitation of higher level electrons in the films. The microprobe was operated in the wavelength-dispersive X-Ray spectrometry (WDS) mode using an electron beam of 6kV. The 6kV beam was used in order to prevent beam penetration to depths greater than $> 0.5\mu\text{m}$. The detection limit for this system is on the order of 100ppm and elements with atomic numbers >5 can be detected. Standards were fabricated InP, InAs, InSb, GaAs, and GaSb wafers and a standard for Tl was made by depositing pure Tl metal on Si⁴⁹.

2.7.4 Auger Electron Spectroscopy

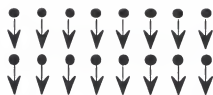
Auger electron spectroscopy was performed on select samples using a Phi 660 scanning Auger multiprobe. Spectra were obtained from both surface scans and depth profiling for the Tl-containing materials. Some estimations of elemental concentrations

were obtained by comparing the Auger electron yields factoring in the different elemental sensitivity factors from the Phi's handbook of Auger electron spectroscopy⁵⁰.

2.7.5 Scanning Electron Microscopy

Epilayer morphologies were examined by a JEOL 6400 scanning electron microscope (SEM). Samples were examined using a 15 kV accelerating voltage and both secondary and backscattered images were obtained. Backscattered imaging was found to be particularly effect for adding contrast to different phases that occur in the growth of the TI alloys.

MBE



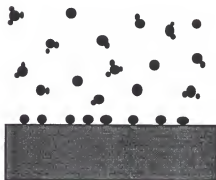
← Group III Atomic Beam



← Kinetic Process

← Substrate

MOCVD



← Partially Pyrolysed Group III Alkyls

← Stagnant Gas Boundary Layer

← Some Pyrolysis

← Substrate

MOMBE



← Group III Alkyl Beam

← Thermal Pyrolysis

← Substrate

Figure 2.1: Arrival and reactions for different epitaxial techniques.

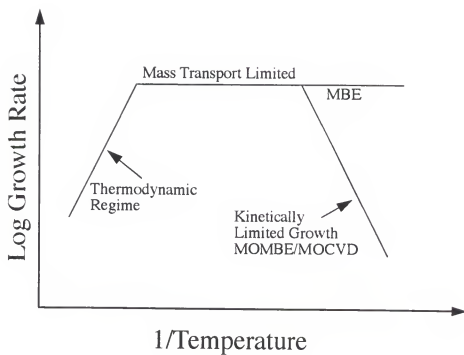


Figure 2.2: Schematic of the growth rate versus temperature for MBE, MOCVD and MOMBE.

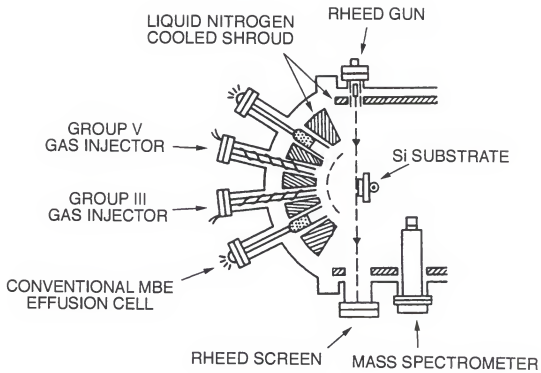


Figure 2.3: Schematic diagram of typical GSMBE/MOMBE growth chamber.

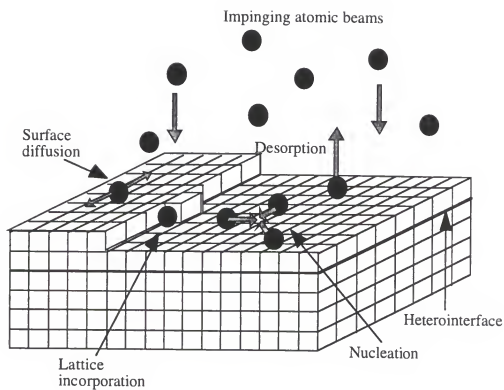
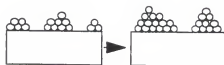


Figure 2.4: Schematic illustration of surface processes occurring during film growth.



Volmer-Weber (VW), island



Frank-van der Merwe (FM), layer-by-layer



Stranski - Krastanov (SK), layer-island

Figure 2.5: The three mechanisms for epitaxial growth.

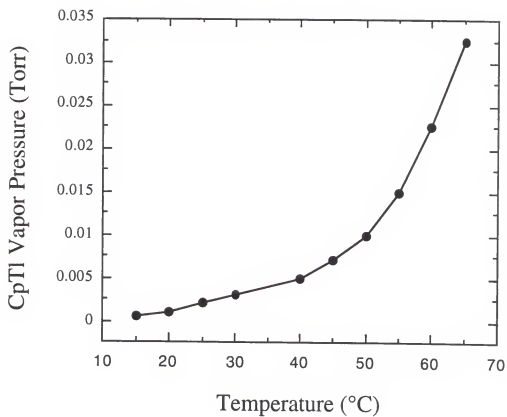


Figure 2.6: CpTl vapor pressure as a function of temperature.

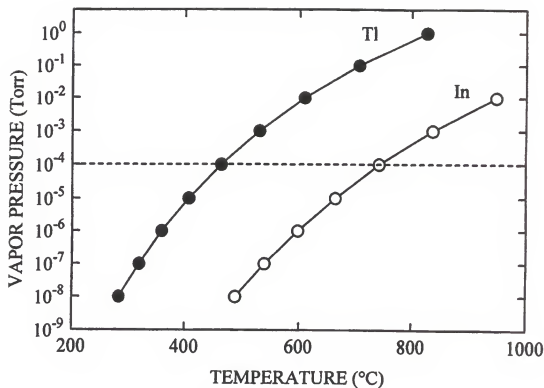
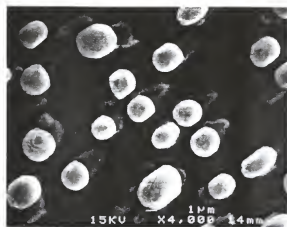


Figure 2.7: Vapor pressure of Tl as a function of temperature. Data for In is shown for comparison. Dashed line represents the pressure used for deposition in GSMBE.



(a)



(b)



(c)

Figure 2.8: (a) SEM photo of a TI droplets on an InP wafer at 350°C, (b) TI droplet on a InP surface at 400°C, (c) same growth conditions as a and b but with a InP substrate temperature of 425°C.

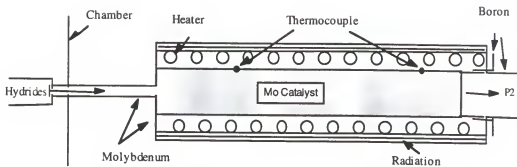


Figure 2.9: Schematic diagram of a low pressure Mo thermal cracker.

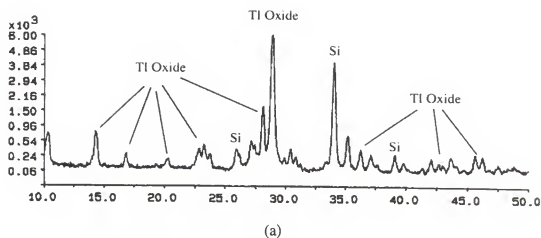


Figure 2.10: (a) x-ray diffraction scan of Tl deposited on a Si substrate and exposed to air for 24 hours, (b) an SEM image of the oxidized Tl droplets surface of the Si wafer.

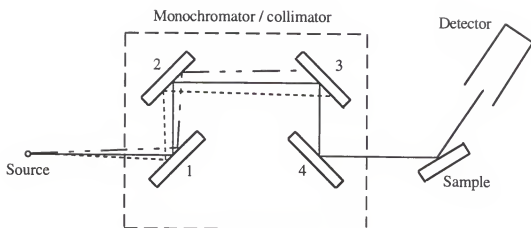


Figure 2.11: A schematic of showing the alignment of the Ge crystals in the monochromator/collimator used in the HRXRD system.

CHAPTER 3 THE THALLIUM CONTAINING PHOSPHIDE SYSTEM

3.1 Introduction

As discussed in Chapter 1, dilation that results from the addition of a larger atom like Tl into a lattice such as InP is one of the ways proposed to fabricate infra-red (IR) detectors^{15,16}. Previous work in the Tl-containing phosphide system has been sparse. At this point, only two other groups have published findings on the epitaxial growth of TIP or the incorporation of Tl into InP. The first such study, by M. Razeghi et al., attempted to form InTIP by MOCVD, and reported a mixture of InP and a TiP_3 phase^{19,51}. The data presented to support this finding was an increase in the photoresponse cutoff wavelength and hall mobility of the InP-TIP₃ two phase material when compared to similarly grown samples without Tl. The second group was H. Asahi et al. at Osaka University^{52,53}. Asahi reported obtaining growth of TIP and $In_{1-x}Tl_xP$ through all Tl concentrations of x ($0 \leq x \leq 1$). Their conclusions were derived from double crystal x-ray diffraction (DCXRD) and reflected high energy electron diffraction (RHEED). This group states further that there is no evidence of phase separation as was reported in the InTlSb system by Huang, Cohen and Stringfellow⁴⁰.

A phase diagram for the Tl-P system can be seen in Figure 3.1. This figure was taken from work prior to the 1950's by Hansen⁵⁴. Although this phase diagram is incomplete, one can see that there is some solubility of Tl in P. The P-rich region, $P \geq$

75%, supports the observations of Razeghi et al., but it should be noted that phase was only produced at high pressures. Hansen further states that Montignie reported in 1937 that the P-rich region shown in the phase diagram may be TiP_3 ⁵⁵. Regions to the left of the P-rich region in the phase diagram appear to be a mix of Ti and the P-rich TiP_x at temperatures below 302°C. This would suggest that it may be possible to form an alloy of Ti and P although not necessarily a zincblende structure. No information regarding the crystal structure or band structures of this TiP_x has been reported.

This chapter will discuss the attempts to grow TIP and InTIP over a variety of growth conditions. An effort will be made to optimize the growth kinetics such that it is favorable for the formation of a stable phase of the Ti-containing phosphide material. Examinations of the behavior of these materials both during growth and post growth will be presented. Finally, comparisons with the relevant literature will be drawn.

3.2 The Binary Ti-P Material System

As Hansen's phase diagram suggests, high P over-pressures are most likely needed for synthesis of Ti-P compounds. To increase the phosphorus over-pressure several of the growth conditions can be adjusted. First, the growth temperature can be reduced significantly thus decreasing the amount of P that is desorbed from the growth surface. This can be done by growing at extremely low growth temperatures (<300°C). Also, the V/III ratio can be increased, usually by increasing the group V flux to the growth surface. In the case of GSMBE this can be accomplished by increasing the group V flow rate. In these two ways, the chance of forming a metastable phase of Ti and P may be enhanced.

3.2.1 The Growth of Tl-P Compounds

The growth of TIP was attempted using elemental Tl and PH_3 . A variety of substrate temperatures, 200 - 525°C, were investigated. It was found that the substrate temperature had no effect on the phases produced, and only affected the Tl sticking coefficient. As the substrate temperatures increase towards 425°C, the Tl sticking coefficient approaches zero.

The effects of Tl and PH_3 flux were also examined. It was found that varying the PH_3 flux by a factor of 20, and the Tl flux by a factor of 26, produced only Tl-rich droplets. As the Tl flux increases, the density of metallic droplets increases. Increasing the PH_3 flux had no effect on the growth products produced. These Tl-rich droplets can be seen in Figure 3.2. The secondary electron image of the surface shows Tl droplets that oxidize readily upon exposure to air and form an oxide with the composition of Tl_2O , indicative of a monovalent Tl state.

Several different substrates were used in order to determine if substrate or substrate orientation would have any effect on the growth of TIP. It was found that substrates of GaAs (100), InP (100), and InP miscuts of 2° and 4° off the (100) had no effect on the Tl and P growth products. Capping these Tl-rich droplets with InP proved to be difficult as can be seen in Figure 3.3. In this SEM micrograph it can be seen that the metallic Tl droplets cannot be capped with InP. Instead, the droplets tend to ride on the growth front as it progresses. In some instances, it may appear that the size of the Tl-rich droplets are decreasing and hence a cap layer is forming around the droplets but, upon careful study at several different temperatures this was found not to be the case. The cap layer is usually grown at temperatures slightly above the unity sticking coefficient of Tl. Thus, droplet density is being reduced by desorption of Tl from the surface during deposition and not by capping. If the capping layer is large enough (grown for a long enough period), droplets will be completely removed from the growth surface and it will appear specular. Auger and

microprobe on these samples show no evidence of significant Tl concentrations in the layer. Furthermore, x-ray diffraction reveals no additional Tl-containing phases nor does high resolution x-ray show any significant increase in the lattice parameter of the capped layer beyond that of normal InP.

3.2.2 Closed Space Vapor Transport

An InTIP sample was grown by A. Sanjurjo and K. Wong at SRI by closed space vapor transport. This growth technique makes use of a sealed ampoule where high phosphorus over-pressures can be maintained. Figure 3.4 shows the resulting surface features as seen by secondary electron imaging. Electron microprobe analysis revealed the presence of a P-rich phase with the approximate composition of TIP_4 . This TIP_4 phase can be seen in the micrograph as the longer, faceted bar-shaped features. Other surface features on the InP include elemental Tl and Tl_2O . The sample was examined using standard x-ray diffraction. Identification of the TIP_4 structure proved to be difficult because of the number of additional x-ray peaks from Tl and Tl-oxides.

Though this p-rich TIP phase is not stoichiometric, its existence is encouraging because it demonstrates some Tl reactivity. This P-rich phase is consistent with the phase diagram of Hansen⁵⁴ and also with the TIP_3 reported by M. Razeghi et al.^{19,51} using MOCVD. One additional reason why the formation of this P-rich TIP phase is significant is that this sample appears to be stable in air indefinitely. The closed space vapor transport sample grown at SRI shows no signs of oxidation for a period of time greater than 2 years.

3.2.3 Summary of the Tl-P Synthesis

All Tl-P samples grown using GSMBE produced metallic Tl droplets for all growth conditions. For substrate temperatures above 325°C, the Tl sticking coefficient decreases

rapidly with increasing temperature until approximately 425°C where there is virtually no deposition of Tl. Upon exposure to air the metallic Tl droplets form crystallites of TlO_x the appear to grow from the surface of the sample. If left in air long enough virtually all of the metallic Tl will oxidize and form Tl_2O . An oxide with this stoichiometry is indicative of Tl in a monovalent state.

The sample grown at SRI using closed space vapor transport and characterized at the University of Florida was found to have a P-rich TlP_x phase. This phase has the approximate composition of TlP_3 as indicated by the electron microprobe. This phase was stable in air for a period of at least 2 years. These results are in agreement with the phase diagram of Hansen and the MOCVD work of Razeghi et al.. Razeghi's MOCVD result of TlP_3 could not be duplicated using GSMBE since the over-pressure of P that can be obtained in MOCVD is greater than what is possible in GSMBE.

3.3 Synthesis of Compounds Containing Indium, Thallium and Phosphorus

Growth conditions for homoepitaxial InP were optimized for In sources of trimethylindium (TMI), triethylindium (TEI), and elemental In. Catalytically cracked PH_3 was the group V source in these experiments. Substrate temperatures that ranged between 200 - 525°C and were used to study the effect of temperature on the In-Tl-P phases produced. The effects of In, Tl and PH_3 flux were also examined. It was found that varying the PH_3 flux by a factor of 20, and the Tl flux by a factor of 15, produced a mixture of InP and Tl-rich droplets independent of the source flux. An example of this characteristic morphology can be seen in the SEM image in Figure 3.5. This secondary electron image of the surface shows metallic Tl droplets in an InP matrix. As was the case for the Tl-P, these droplets oxidize readily upon exposure to air. The accompanying micrographs in Figure 3.5 are an indium x-ray map and a thallium x-ray map respectively. The x-ray maps of the Tl and In are of the same area of the sample the secondary image so

that the can be directly compared. The In x-ray map shows areas clearly deficient of In where the droplets appear on the surface. The Tl x-ray map shows a wider distribution of Tl across the surface with it most heavily concentrated in the areas of the large droplets. It is believed that the Tl present between the large droplets are smaller droplets of Tl that have yet to coalesce into the large droplets.

Figure 3.6 shows samples grown under identical conditions other than Tl cell temperature. Figure 3.6 (a), (b) and (c) were grown at cell temperatures of 525°C, 540°C and 560°C respectively. The SEM images in this figure illustrates the formation of Tl droplets in an InP matrix. Several different substrates were used in order to determine if substrate or substrate orientation would have any effect on the phases produced. It was found that substrates of GaAs (100), InP (100), and InP miscuts of 2° and 4° off the (100) had no effect on the formation of the In, Tl and P growth products. Once again capping these metallic Tl droplets with InP proved to be difficult. The droplets ride on the growth front as it progresses. This is strong evidence that Tl has a tendency to surface segregate.

3.3.1 Efforts to Suppress Droplet Formation

In an effort to suppress droplet formation, several superlattice structures were grown consisting of alternating layers of InTlP and InP. These layers were deposited by shuttering the Tl cell open and closed in 15 sec intervals for a total growth time of 40 minutes. This layer was followed by the growth of a 10 minute InP cap. The surface morphology of this sample revealed some evidence of oxide formation but less than InTlP samples grown under similar but non-superlattice conditions. The reduction in the droplet density was believed to be more from a reduced amount of Tl in the layer from shuttering the Tl and as discussed previously, the desorption of Tl from the surface as the cap layers is being grown. A sample grown with a substrate temperature of 350°C was examined using cross-sectional transmission electron microscopy. Other than a high density of

micro-twins, no evidence of any superlattice structure such as imaging contrast that should be present due to the different atomic weights of these alternating InP and InTlP layers was found. When an EDS probe in the TEM was used no detectable Tl was present in the layer. The fact that micro-twins were present in this layer but not in a layer grown under the same conditions without Tl, suggests that there is either some small amount of Tl incorporation (possible at undetectable levels but enough to cause defect formation) or that the Tl segregates so badly on the surface that it causes stacking sequence interruptions that lead to the formation of micro twins.

During the course of these experiments, further attempts to force Tl to incorporate in the lattice were attempted. One such attempt was the use of Sb as a surfactant. incorporation of Sb is known to be less than that of P and typically strongly segregates. It was believed that if the Sb had a higher propensity to segregate than Tl and if segregation and not solubility was the limiting factor for incorporation of Tl into InP, that a flux of Sb during growth might aid in the incorporation of Tl. SEM showed the surface morphology of this sample to be rough with what appeared to be droplets. Examination using EMP shows that the droplet formation on the surface were actually a phase of Tl and Sb. Although using Sb as a surfactant was not successful in producing InTlP, the formation of a TlSb phase was a strong indicator that Tl has at least some solubility in the antimonide system. The formation and characterization of this phase will be presented in depth in Chapter 5.

3.3.2 Comparison of InTlP With Published Results

Only two groups have published reports on the fabrication of InTlP. The First is M. Razeghi at Northwestern who reported that they could only produce a two phase mixture of TlP_3 and $\text{InP}^{19,51}$. This was discussed previously in this chapter. The second report is from H. Asahi et al. at Osaka University, Japan^{52,53}. Asahi's work reports the

formation of InTIP throughout the entire compositional range when using growth temperatures of 400° - 450°C. Asahi's results were obtained in a GSMBE system very similar to the one used to produce the majority of samples presented in this dissertation. A similar growth regime has not proven successful in producing TIP or InTIP in our system as was reported by Asahi.

To further investigate Asahi's findings, samples were grown with as similar growth conditions as similar to Asahi's as possible. The sample consisted of three layers; a 2000Å buffer layer of InP, one hour of TIP, and a 4000Å cap layer of InP. The resulting surface morphology as seen by SEM is shown in Figure 3.7. The surface morphology of this sample is smooth and featureless, indicating that there has been a good quality growth. This is in agreement with Asahi. However, one of the first things that was noted with our "TIP" sample is that the thickness of the entire layer as measured by a profilometer, was only as thick as the estimated thickness of the cap and the buffer layer combined. This suggested that if any "TIP" had grown, the growth rate was very slow and the layer very thin.

Analysis of these layers were carried out by x-ray diffraction. Figure 3.8 is the DCXRD from Asahi et al⁵². It can be seen that there is a separation of 278 arc-sec between the InP substrate peak and what Asahi has labeled the TIP layer peak. For comparison the sample grown mimicking Asahi's growth procedure is presented in Figure 3.9. This figure taken from a 5-crystal HRXRD shows three peaks; a substrate peak, a buffer layer peak and an epilayer peak. The separation between the buffer and epilayer peaks are 593arc-sec. This is a little more than twice the separation found in Asahi's work. However, EMP analysis was unable to detect any Tl in the layer up to it's detectivity limit of approximately 1%. This may be understandable because the EMP has a penetration depth of approximately 0.5µm and the cap layer was estimated at 0.4µm. Both Auger electron spectroscopy (AES) and secondary ion mass spectrometry (SIMS) were used to give depth profiles of our sample. AES showed no evidence of Tl to the detectable limits of

approximately one atomic percent. The SIMS results are presented in Figure 3.10, which shows that Tl is only present in this sample to a concentration on the order of 10^{16} atoms/cm³. One should also note that though there is a substantial amount of As in the film the concentration is not high enough to account for the large lattice shift.

Since the Tl-P and Tl-In bond lengths are not known we are unable to determine what the theoretical strain should be in these samples. From the XRD comparisons and the AES and SIMS it is clear that our sample has more strain than Asahi's but has no substantial amount of Tl present. It is believed that metallic impurities present in these samples may be responsible for the increased amount of strain found. All of this data which includes XRD, SIMS, EMP and AES combined with the fact that no substantial increase in thickness was obtained from a profilometer over the combined thicknesses of the cap layer and the buffer layer, indicates only insignificant amounts of Tl.

3.4 Summary of the InTIP Ternary Alloy System

All samples grown using GSMBE produced Tl-rich droplets in a matrix of InP under all growth conditions and substrates. The density of these Tl-rich droplets and their oxidation behave in the same manner as described previously in the TIP binary section. InTIP could not be formed as an alloy nor in a two phase mixture of InP and TIP₃. This behavior was not in agreement with that reported in the literature. The mixture of TIP₃ and InP found under certain growth conditions by Razeghi using MOCVD, is consistent with an early phase diagram by Hansen that indicates a P-rich phase forms under a high over-pressure of phosphorus. The pressures obtainable in MOCVD are higher than in GSMBE and thus may explain the different products formed. To compare with the work by Asahi, which reports the formation of stoichiometric TIP and InTIP throughout all compositions of Tl using GSMBE, experiments were duplicated with some similar XRD results. However, these samples under careful study were found to contain no significant amounts of Tl when depth profiling was carried out with AES and SIMS.

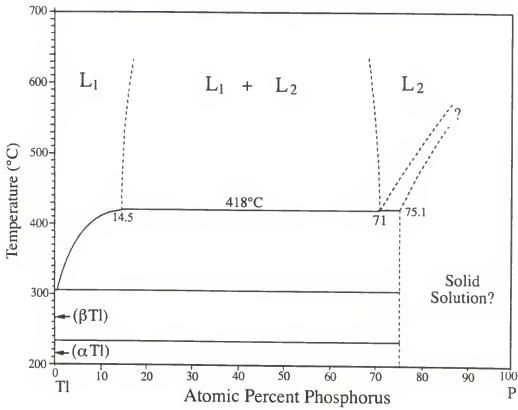


Figure 3.1: Phase diagram of the Tl and P binary system. Redrawn from reference (54).



Figure 3.2: SEM image at 4,000x of partially oxidized Tl droplets formed on an InP substrate during attempted TIP formation.

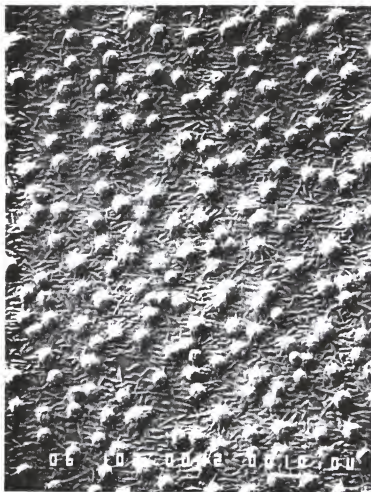


Figure 3.3: Secondary electron image of partially oxidized TI droplets grown in an attempt to form TIP at a substrate growth temperature of 400°C with an additional 20 minute InP cap at a magnification of 1,000x.

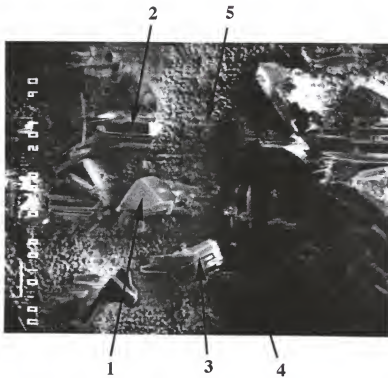
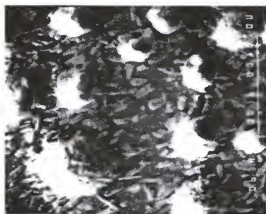
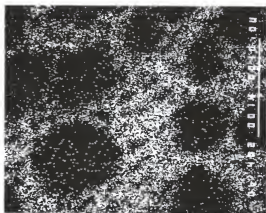


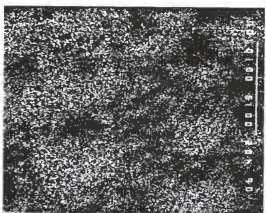
Figure 3.4: SEM image of sample grown by closed space vapor transport at 1,000X. Numbering of arrows correspond to the P/Tl ratio as determined by EMP analysis. (1) 4.7, (2) 5.2, (3) 4.4, (4) 2.7, (5) a mixture of InP, Tl and TlO_x .



(a)

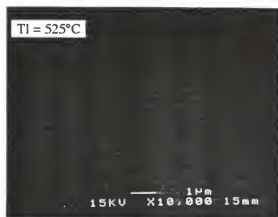


(b)



(c)

Figure 3.5 SEM image of InTIP sample (a), with corresponding (b) In x-ray map, and (c) TI x-ray map. All magnifications are at 4,000x.



(a)



(b)



(c)

Figure 3.6: SEM images of InTIP as Tl cell temperature is increased from (a) 525°C, (b) 540°C, and (c) 560°C. All magnifications are at 10,000x.

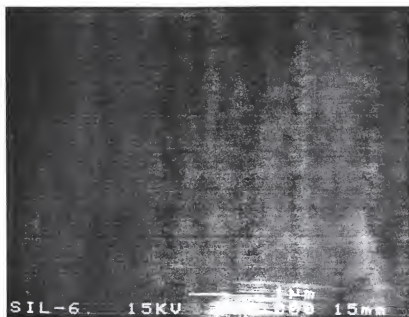


Figure 3.7: SEM image at 10,000x of a structure consisting of 2000Å InP buffer and 6000Å InP cap surrounding layer grown with only elemental Tl and P for one hour.

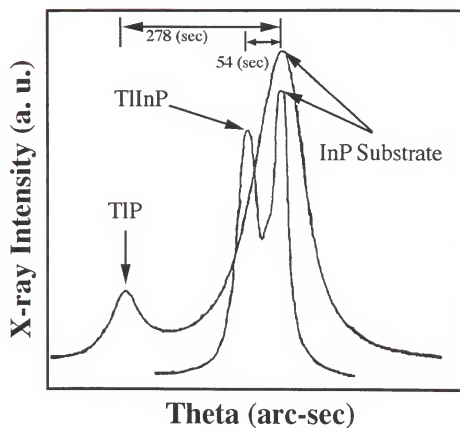


Figure 3.8: Double crystal x-ray diffraction of TIP and InTIP layers grown by Asahi. Figure redrawn from reference (52).

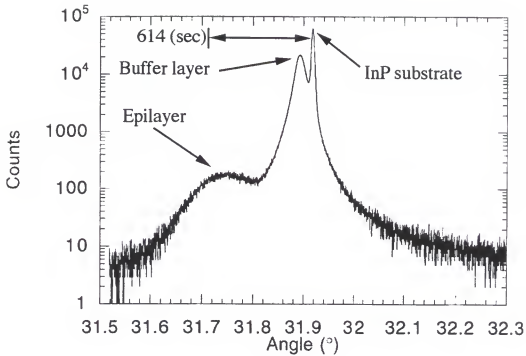


Figure 3.9: High resolution x-ray diffraction of structure consisting of 2000Å InP buffer and 6000Å InP cap surrounding layer grown with only elemental Tl and P for one hour. The separation between the buffer and the epilayer is 593 arcsec.

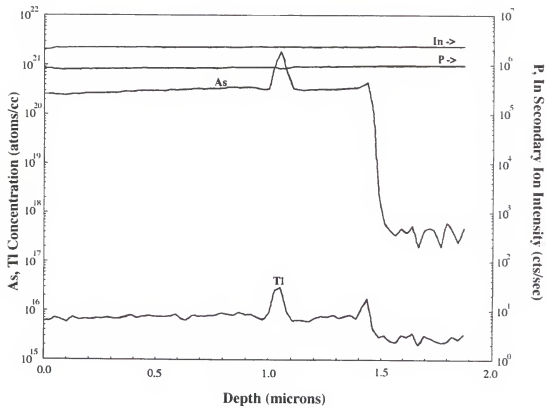


Figure 3.10: Corresponding SIMS of structure consisting of 2000Å InP buffer and 6000Å InP cap surrounding layer grown with only elemental Ti and P for one hour. SEM and x-ray data shown in Figure 3.6 and Figure 3.8 respectively.

CHAPTER 4 THE THALLIUM CONTAINING ARSENIDE SYSTEM

4.1 Introduction

The thallium containing arsenides were examined extensively in this dissertation. In general, the arsenide system tends to be a more robust system which should ease some of the difficulties in the processing of InP based materials. The amount of Tl needed in the InTlAs system is about a quarter of the amount of Tl needed in InTlP to achieve the target bandgap of 0.1eV. The composition estimated to correspond to this 0.1eV bandgap is $\text{In}_{0.85}\text{Tl}_{0.15}\text{As}$ as estimated by M van Schilfgaarde et al. at SRI¹⁶. At an incorporation of only 15% Tl, as opposed to 67% Tl as is estimated for the InTlP system, it is much more likely that potential problems such as segregation can be overcome by growth in a metastable regime. Other than the author, there has been no literature found on the growth or attempted growth of Tl- and As, and/or In-, Tl- and As-containing materials by any growth mechanism.

A phase diagram of the Tl-As system is presented in Figure 4.1. This is a figure that was redrawn from the work of Hansen⁵⁴. As can be seen in the figure, there is little (if any) solubility of Tl in As or vice-versa. Although the phase diagram presented does not represent constant pressure conditions, it is believed that this system will change only slightly with minor changes in pressure even at temperatures as high as 600°C. Unlike the Tl-P phase diagram presented previously in Figure 3.1, the Tl-As system is not believed to have any regions of Tl and As containing solid solutions. No other more recent phase

diagrams could be found of the Tl-As system nor could any phase diagrams be found of the ternary InTlAs system. The effect of adding In to the Tl-As phase diagram is unknown but a limited amount of solubility is expected. Whether this solubility will be enough to satisfy the 15% incorporation estimated to be needed for this system is yet unknown.

This chapter will discuss attempts to fabricate both the binary TlAs and the ternary InTlAs systems over a wide variety of growth conditions. An effort will be made to optimize the growth kinetics such that it is favorable for the formation of a stable phase of a Tl-containing arsenide material. Examinations of the behavior during growth and post growth environments will be presented.

4.2 The Growth of Tl-As Compounds

The growth of TlAs was attempted using elemental Tl and AsH_3 . A variety of substrate temperatures ranging from 200 - 450°C were used to determine the effect on the Tl-As phases produced. It was found that the substrate temperature had no effect on the phases produced, and affected only the sticking coefficient of Tl. As was the case in the Tl-P system, as the substrate temperature increases towards 425°C the sticking coefficient rapidly approaches zero. The sticking coefficient of Tl was discussed more extensively in Chapter 2 and Chapter 3.

The effects of Tl and AsH_3 flux were also examined. It was found that varying the AsH_3 flux by a factor of 15 and the Tl by a factor of 25 produced only Tl-rich droplets. As the Tl flux was increased the amount of Tl-rich droplets on the surface also increased. As the group V flux was increased, in this case by increasing the AsH_3 flow, no changes could be found in the products produced. A representative secondary electron image of the of the Tl-As morphology can be found in Figure 4.2. One can see the faceted nature of the droplets and the spiral defects that appear on the surface of the droplets. It should be noted that the Tl-rich droplets, containing less than an atomic percent of As,

appear to have a reduced reaction with exposure to air when compared to those formed under a phosphorus over-pressure. This reduced reaction is not dramatic but these Tl-rich droplets can be exposed to air for a few minutes longer without the onset of oxidation.

Several different substrates were used in order to determine if substrate or substrate orientation would have any effect on the growth of "TlAs". It was found that substrates of GaAs [(100)] and InP [(100), (111) and (311B) as well as 2° and 4° miscuts from the InP (100)], have no effect on the Tl and As growth products. From EMP analysis, we find that the droplets formed have essentially the same Tl-rich composition and do not appear to be affected in any capacity by a change in substrate orientation.

Once again capping these layers was unsuccessful. In this case, attempted capping of "TlAs" with InAs resulted in the same type of segregation problems that arose in the Tl-P system. Tl tends to ride on the growth front as the InAs layer is progressing, indicating a high propensity for surface segregation. As was the case in the Tl-P system, the surface loses Tl if the capping layer is grown at temperatures which result in a low Tl sticking coefficient. Alternative attempts to encourage the Tl to bond covalently with a group V element such as As were also unsuccessful. It was thought that attempting Tl-As growth in the presence of an RF or ECR He plasma could provide the energy necessary to force the electrons in the s orbital to hybridize and thus participate in bonding. Unfortunately this approach did not produce any change in the Tl and As growth products.

4.3 Summary of the Tl-As Binary Alloy

As was the case in the binary Tl-P system examined in Chapter 3, the Tl-As system produces Tl-rich droplets on the surface of the respective substrate used in the experiment. These droplets form and appear to be independent of growth temperature, Tl flux, substrate orientation and group V flux. These Tl-rich droplets that are produced oxidize rapidly upon

exposure to air and form an oxide with the composition roughly of Tl_2O that is indicative of Tl in the monovalent state.

4.4 Indium, Thallium and Arsenic Containing Ternary Alloys

Growth conditions for elemental In were optimized for the growth of InAs. Catalytically cracked AsH_3 was employed as the group V source in this experiment set. Substrate temperatures ranged from 200 - 425°C and were used to study the effect of substrate temperature on phases produced. The group III fluxes of In and Tl were varied by a factor of 10 and 15 respectively and the group V flux was varied by a factor of 15.

The effect of different substrates such as GaAs (100), GaSb (100), and InP (100), (111), (311B) were also studied. Figure 4.3 shows an example of the different substrate orientations on the growth products of Tl droplets in an InAs matrix under identical growth conditions. As can be seen in this figure, the different substrate orientations only affect the droplet orientation that forms on the surface. From EMP analysis, we find that the droplets formed have essentially the same Tl-rich composition and do not appear to be affected in any capacity by a change in substrate orientation. One further note that should be mentioned is that the oxidation rates appear to be fastest in the (111) orientation and slowest in the (100) substrate orientation.

Substrate growth temperature in this system proved to produce three major growth regimes. The first occurs at temperatures between ~ 400 - 425°C. This regime produces a mixture of InAs and Tl droplets. As was the case in the InTIP system, the matrix, in this case InAs, contains less than 1% of incorporated Tl. The droplets that can be found on the surface are composed primarily of Tl and have concentrations of In and As below the detection limit of the electron microprobe (<1%).

As the substrate temperature is decreased to approximately 375°C, a mixture of two phases begins to appear. A backscattered electron image of an InTlAs sample grown under

these conditions can be seen in Figure 4.4. Backscattered electrons were used for imaging in this micrograph to highlight the different phases. As is labeled in this figure the darker or lower atomic weight material is InAs, while the lighter contrast material is a phase containing substantial amounts of both Tl and As. Electron microprobe analysis of this sample determined this phase to have an approximate composition of Tl_7As_2 .

Typically segregation is overcome by reducing the growth temperature. Thus it is not surprising that by reducing the growth temperature to 275°C , the growth products are once again changed. In this regime, the sample consists of an InAs matrix with Tl droplets and some regions of InTlAs. These phases can be easily distinguished because the Tl droplets oxidize rapidly into small crystallites while the InTlAs regions have a reduced rate of oxidation. The sample morphology is presented in Figure 4.5 as seen by SEM. Figure 4.6 is the corresponding AES depth profile. The AES profile in these regions of InTlAs have flat profiles throughout the islanded InTlAs region. These profiles are much flatter than those measured in the capped film grown at 375°C , and the thickness of the Tl-rich near surface region has been greatly reduced. The composition of this InTlAs alloy was determined based on the sensitivity factors for In, Tl, and As. These sensitivity factors are 0.97, 0.42 and 0.12 respectively yielding an estimated concentration of approximately $\text{In}_{0.65}\text{Tl}_{0.35}\text{As}$ and appears to be stoichiometric with a difference in the group III and group V totals of only about 1%. This provides some compelling evidence that in the InTlAs system segregation may in fact be responsible for much of the unusual growth behavior. AES profiling in the matrix found no significant concentrations of Tl. Depth profiling the oxidizing droplets produced primarily Tl with decreasing oxygen content as sputtering continued. This InTlAs phase is difficult to reproduce and is highly dependent on V/III ratios as well as on substrate temperature.

Oxidation of the Tl- and As-containing phases occurs at a slower rate than the predominately Tl-containing phases. Complete oxidation of the "TlAs" and "InTlAs" phases occurs in about 24 hours. An example of the oxidation of these samples is shown

in Figure 4.7. Figure 4.7(a) is an SEM micrograph of Tl-rich droplets in an InAs matrix. This sample was left in air for 24 hours and subsequently dip etched in hydrofluoric acid to remove the oxide layer. The resulting morphology is shown in Figure 4.7(b). The Tl-rich droplets have oxidized and subsequently been removed by the HF dip etch leaving pits on the surface in the areas once occupied by the Tl droplets.

Capping InTIAs proved to be difficult as it was in the InTIP system. Figure 4.8 shows an SEM image of a sample that was grown at 375°C and subsequently capped with InAs for 10 minutes. The corresponding AES depth profile is shown in Figure 4.9. As can be seen in these figures, there are still large amounts of Tl-rich material in the near surface region. The amount of Tl decreases upon further sputtering into the sample while the amount of As and In increase. It is not conclusively known if this is due to severe surface segregation indicating at least partial success of the capping layer or if we are merely probing a small Tl droplet and are inadvertently collecting data from the surrounding InAs matrix or capped layer.

4.5 Summary of the InTIAs Ternary Alloy System

The InTIAs system has produced two new phases of Tl-containing materials never before described in the literature. These phases were created by effectively reducing the substrate growth temperature and hence, reducing the amount of Tl segregation. The first of the two new phases was produced at a substrate temperature of about 375°C. This proved to be a Tl-rich phase with the approximate composition of Tl_7As_2 . Characterization of this phase proved difficult due to several factors including rapid oxidation, and the fact that this phase only forms in the presence of both elemental Tl and InAs. The existence of this Tl- and As-containing phase does not appear anywhere in Hansen's binary phase diagram.

A second novel phase was formed by decreasing the substrate temperature to 275°C producing a mixture of In, Tl, and As. Characterization was difficult in this phase also, due to its instability, but AES confirmed an InTlAs phase along with Tl droplets in an InAs matrix. AES determined the composition of this phase to be $\text{In}_{0.65}\text{Tl}_{0.35}\text{As}$ and was stoichiometric to within 1% of group III and group V totals. Due to the inherent instability of this compound in air and combined with the fact that these materials can not be formed without the presence of pure Tl droplets and InAs, any optical characterization proved to be ambiguous. There is clearly a strong influence of the substrate temperature and V/III ratio in producing In, Tl and As containing phases. However, under exacting conditions, what appeared to be a stoichiometric InTlAs phase was produced indicating that the surface segregation and not solubility may be the major hurdle to overcome in this system.

4.6 Modification of Tl-containing Phosphide and Arsenide Theory

Modification of the Tl-based III-V materials were examined due the discrepancies between the theory predicted by SRI and the experimental results presented here. In previous work SRI stated that the Tl-containing III-V's were predicted to be better bound than HgCdTe for compositions corresponding to the absorption in the LWIR. Although those findings are still valid for the cohesive energies, some key thermodynamic properties were overlooked⁴¹. Therefore, these thermodynamic properties were studied pertaining to the growth of zincblende TIP, TlAs, InTIP and InTlAs. It was predicted using the local density approximation (LDA), that both TIP and TlAs should be unstable with respect to decomposition into the elemental constituents (Tl, and P or As respectively) except at very high group V over-pressures. Further calculations indicate that a small amount of Tl incorporation in InP and InAs respectively should be possible²¹.

The phase stability, phase transitions and vapor pressure all depend on the free energy of the system. SRI found that InTIP and InTlAs have negligible mixing energies

hence, only the entropy terms were included in the calculations of the alloys free energy calculations. The addition of a mixing energy term will only slightly change the predicted partial pressures over the solid alloy at a given temperature. Because of the positive excess energies calculated for TIP and TIAs, SRI results indicate that there is no existence regions for these compounds, however assuming conservative errors in the LDA, formation of a metastable phase may still be possible. The partial pressures of the anion dimers and tetramers over the alloys for several temperatures is shown in Figure 4.10. The LDA predicts in the ternary InTl- P or As cases that only a small amount of Tl incorporation will be obtained unless extremely high group V over-pressures are employed during growth. SRI predicts that only 5% Tl incorporation is possible in InTlP at a substrate temperature of 350°C, far less than the 67% Tl needed for the LWIR applications. Although only a small amount of Tl is predicted to incorporate in InTIAs, the additions of error estimations may make the attainment of the 15% Tl needed in the arsenide system. Based on these new thermodynamic calculations, growth of the InTlP and InTIAs alloys will be extremely difficult without the use of a high pressure system²².

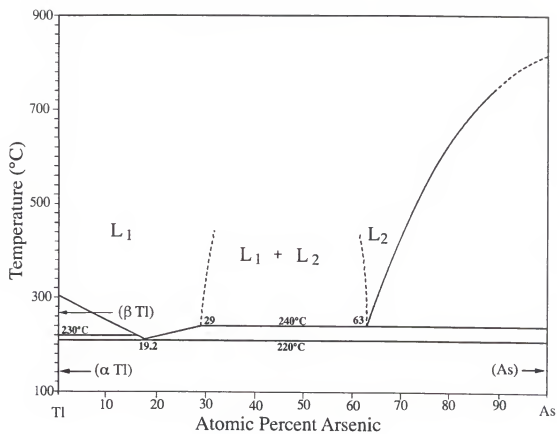


Figure 4.1: Phase diagram of the Tl-As binary system. Redrawn from reference (54).

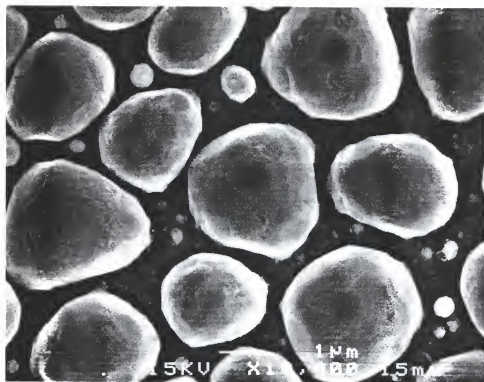


Figure 4.2: Representative SEM image of TI droplet formation on an InP substrate during the attempted growth of TIAs.

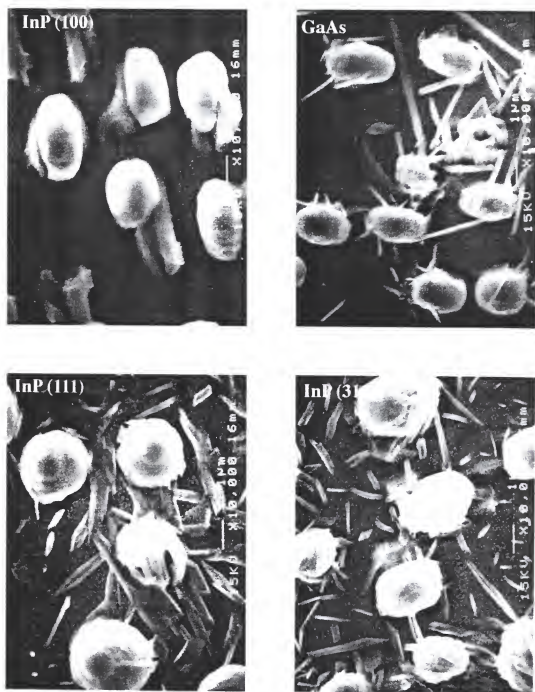


Figure 4.3: SEM micrographs of TI-As grown using identical conditions on InP (100), GaAs (100), InP (111), and InP (311b) substrates. All magnifications are at 10,000x.

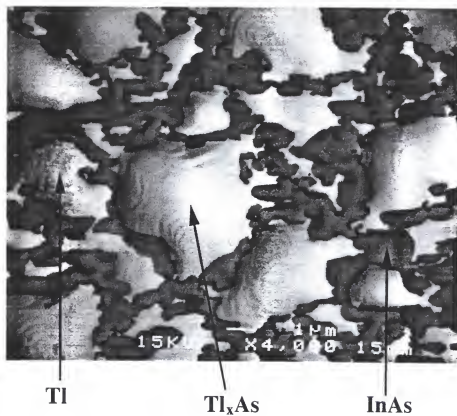


Figure 4.4: Backscattered electron image of InTlAs sample grown at 375°C. Lighter contrast regions denote a significant amount of Tl while darker area is InAs ($x \sim 3.5$).

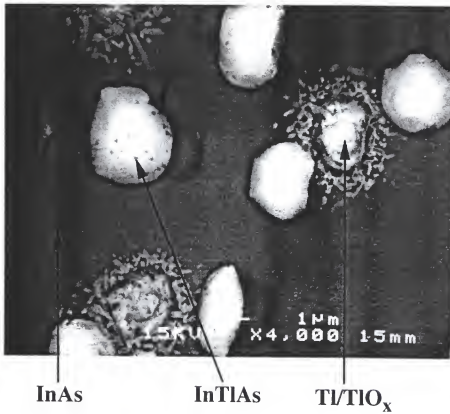


Figure 4.5: SEM image of InTlAs sample grown at 275°C. Three main phases present are Tl, InAs, and InTlAs. Note the visible difference in the oxidation between Tl and InTlAs phases.

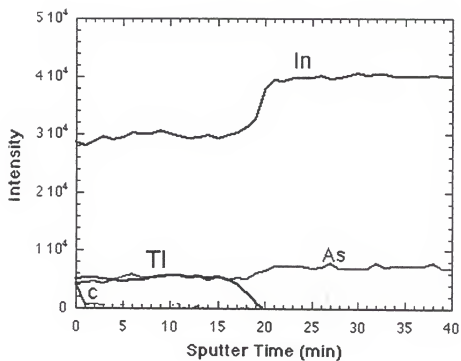
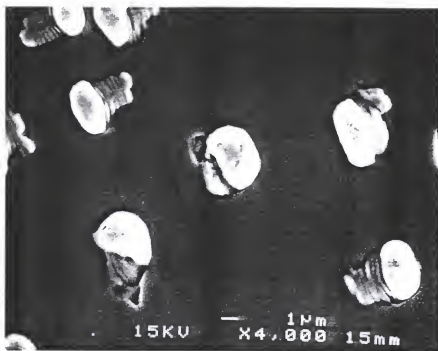


Figure 4.6: Auger depth profile of an InTlAs region shown in Figure 4.5.



(a)



(b)

Figure 4.7: InTlAs sample grown at 375°C (a) as grown and (b) after two weeks in air and an HF dip etch to remove oxide formation.

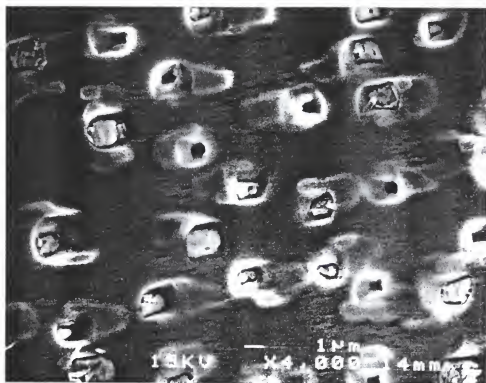


Figure 4.8: InTlAs sample grown at 375°C and subsequently capped for 10 minutes with InAs. Magnification is 4,000x.

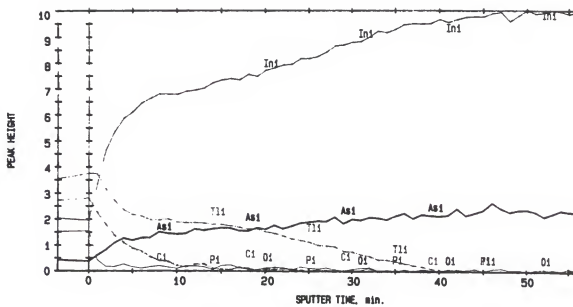


Figure 4.9: Auger depth profile of capped InTlAs sample shown in Figure 4.8.

CHAPTER 5 THE THALLIUM CONTAINING ANTIMONIDE SYSTEM

5.1 Introduction

The vast majority of experimental research on the Tl-containing III-V materials has been in the antimonide system. Chapter 1 catalogued results from several groups on the formation of InTlSb alloys. This included one early report from Wood et al. using MBE, which claimed a small incorporation of Tl (~ 5%) but could not accurately quantify the concentration due to a lack of standards²⁵. Wood indicated that the apparent Tl concentration might be a consequence of Tl-Sb liquid accumulation on the surface during growth which then solidifies upon cooling from the growth temperature. The second group with experimental work in the Tl-containing antimonides was Y.H. Choi et al. at Northwestern University using low pressure metalorganic chemical vapor deposition (LP-CVD)^{18,26}. Choi et al. report the growth of some unknown composition of $\text{In}_{1-x}\text{Tl}_x\text{Sb}$ and substantiates their findings with DCXRD and some electrical measurements. DCXRD measurements indicated a shift in the lattice strain towards compression which is unusual for the addition of a larger atom to the lattice. Electrical measurements showed a slight enhancement of the hall mobilities and small shifts in the absorption edge.

To date there have been no published reports on the formation of binary TlSb by modern electronic materials growth techniques. However, a phase diagram of the Tl-Sb binary system can be seen in Figure 5.1^{9,10,54,56}. This phase diagram indicates that there

is an intermediate phase, Tl_7Sb_3 , that can be formed peritectically at temperatures below 226°C^{29} . It is believed that this phase is of the $\text{CsCl}^{29,57}$ crystal structure although some believe it to have a complicated cubic structure^{58,59}. Towards the Tl rich side of the phase diagram one finds a mixture of this phase with elemental Tl and towards the Sb rich side this phase is found with excess Sb.

In the case of the ternary InTlSb , there have been two additional reports of growth since the start of this research. The first is N.H. Karam et al. at Spire who report that InTlSb films were grown successfully at concentrations up to and including 10% Tl using MOCVD⁶⁰. Supporting data presented to substantiate these claims include x-ray diffraction which is similar to the biaxial compressive stress to the lattice observed by Choi et al. (indicating that the bond length of Tl-Sb must be smaller than that of In-Sb despite Tl being a larger atom) and absorption measurements showing response beyond that of InSb. AES was performed indicating Tl on the surface of these films but no depth profiling was shown. Similarly, RBS was employed for the estimation of the Tl content in these films but showed the largest amounts of Tl to be close to the surface of the as-grown film. Karam et al. indicated that this was due to surface segregation of the Tl but this was only observed in the InTlSb films with high Tl contents.

The second report recently published was that of K.T. Huang et al. from the University of Utah. Huang et al. reported that the growth of InTlSb was also attempted by MOCVD⁴⁰. EMP analysis indicated less than 1% Tl incorporation into InSb. Huang found that Tl and Sb accumulate on the surface of the layers, much as described by Wood et al.. From EMP data showing secondary electron imaging of the surface combined with x-ray maps of Tl, In and Sb it was determined that there are regions of Sb-rich and Tl-rich material on an InSb matrix.

Both Huang and Karam have attempted growth of InTlSb using similar growth mechanisms and similar growth conditions. However, they have reported substantially different results. This chapter will detail attempts to grow both the binary compound TlSb

and ternary compound InTlSb by GSMBE. Examination of the behavior of these materials during both growth and post growth environments will be examined. Comparisons with the existing literature will be discussed and conclusions drawn. Finally, a model to explain the behavior of Tl in III-V materials will be presented.

5.2 The Growth of Tl-Sb Compounds

The growth of binary Tl-Sb compounds was carried out using elemental Tl and elemental Sb. The hydride form of antimony, stibine (SbH_3), was not used due to the instability of this source molecule. The synthesis of this material system was studied by varying several different growth parameters including substrate, substrate orientation, V/III ratio and substrate temperature. The results of these different growth parameters are listed below.

In contrast to the arsenides and the phosphides, the Tl-Sb compounds are predicted to have significantly lower group V vapor pressures⁴¹. Thus it was not surprising that Tl was found to react much more readily with antimony allowing a Tl-Sb phase to be obtained at substrate temperatures as high as 400°C. Figure 5.2 is a backscattered electron image of a typical attempt to form the binary TlSb phase. This microstructure was formed on a GaAs substrate at 375°C producing an egg-like structure that consists of a non-enclosing shell surrounding a yolk-like droplet. Backscattered imaging helps distinguish the two different phases by "Z" contrast. The lighter phase or the shell-like form was found to be Tl_7Sb_2 as observed by EMP. The darker phase was found to be elemental Sb that forms under the Tl_7Sb_2 phase. These phases were confirmed with powder x-ray diffraction which shows the Tl_7Sb_2 to have a complicated multi-atom per lattice point, CsCl type structure²⁹.

Further examination of Figure 5.2 shows smaller egg-like phases. As the growth time increases the size of the egg-shaped two phase mixture also increases. It is believed

that the two-phase mixture is most likely a liquid during growth that solidifies during the cooling of the sample from the growth temperature. These small two phase liquid droplets appear to form randomly on the substrate and as the growth progresses the egg-shaped mixtures tend to coalesce, forming a larger egg-shaped mixture of Ti_7Sb_2 and elemental Sb.

This phase mixture was found to clearly be the preferred form of Ti-Sb based on observations of samples grown under a wide variety of growth conditions and on several different substrates. Figure 5.3 illustrates the subtle changes that occur when this two phase mixture is grown on (a) (100) GaAs, and (b) (100) GaSb under identical growth conditions. The differences in the morphologies of the GaAs and GaSb substrates arises from the greater ability of the Ti_7Sb_2 and the elemental Sb to wet to Sb-containing substrate. Thus the Ti-Sb material grown on GaSb substrates tend to be flatter, but still contains the same growth products as were formed on the GaAs substrate. Growth of the Ti_7Sb_2 phase on (100) InP substrates produced a very similar morphology to that found on GaAs.

The effect of V/III ratio was also examined in this experiment set. It was found that increasing the Ti flux produced more Ti_7Sb_2 if sufficient Sb was provided at the growth surface. In all cases the Ti_7Sb_2 phase was not formed without the presence of excess Sb. Furthermore no excess Ti droplets were formed with the Ti_7Sb_2 when a sufficient Sb flux was employed during growth. Figure 5.4 is an example of a material grown under a higher Sb flux than those in Figure 5.3. The major difference arises in the amount of excess Sb that is retained on the surface of the sample. The higher the Sb flux, the higher the amount of Sb on the surface. Changing the group III flux only effects the amount of Ti_7Sb_2 obtained while changing the group V flux only changes the amount of excess Sb.

The Ti_7Sb_2 phase oxidizes more slowly than those phases produced by GSMBE in either the arsenide or the phosphide systems. Figure 5.5 shows the changes that occur in the Ti_7Sb_2 phase as it is exposed to air. Figure 5.5(a) is a typical Ti_7Sb_2 and Sb two phase mixture as described earlier in this Chapter that has been kept under vacuum until the SEM

micrographs could be obtained. Figure 5.5(b) is the same sample after it has been left in air for two days. As one can see, Tl-oxide crystallites have formed on the surface of the Tl_7Sb_2 . Two days of exposure to air is generally enough time for the Tl droplets and phases in the arsenide and phosphide systems to fully oxide (depending on the size of the Tl containing phases, naturally the larger the more time needed to oxidize). Figure 5.5(c) is the same sample after it has been exposed to air for one month. Because the Tl-oxide charges and makes SEM imaging difficult, this particular sample was given a 5 second dip etch in a 1:1 solution of HF and distilled water. The HF solution is not known to etch Tl or any Tl-V compounds but rather removes the Tl-O species. In this case all of the Tl_7Sb_2 has been removed leaving the center droplet of Sb. The typical square-shaped face of Sb can still be seen but the Tl_7Sb_2 phase that once covered it has been removed.

Capping of the Tl_7Sb_2 phase with InSb proved to be unsuccessful. The Tl_7Sb_2 and excess Sb tend to ride on the surface as in the arsenide and phosphide systems. Attempts to form superlattice structures of Tl_7Sb_2 / InSb at several different temperatures resulted in an accumulation of Tl_7Sb_2 and excess Sb on the surface in a matrix of InSb.

5.3 Summary of the Tl-Sb Binary System

The binary Tl-Sb system was examined with respect to group III flux, group V flux, different substrates and substrate temperatures. It was found that the Tl_7Sb_2 phase is the preferred phase in this material system. The Tl_7Sb_2 phase forms under all growth parameters and substrates provided that sufficient group III and group V fluxes are present. This Tl_7Sb_2 phase completely oxidizes in a few weeks. Attempts to cap the Tl_7Sb_2 phase with InSb were unsuccessful.

5.4 Indium, Thallium and Antimony Containing Ternary Compounds

The behavior of Tl in the ternary InTlSb system is much the same as that found in the binary Tl-Sb compounds. Figure 5.6 is a secondary electron image of the typical morphology obtained when attempting to form InTlSb. One can see in this figure that there are clearly phases similar to that found in the binary TlSb system. In fact XRD showed the same phases to be present but in the ternary InTlSb case, additional peaks are found corresponding to InSb. Thus, EMP analysis confirmed the existence of a two phase mixture of Tl_7Sb_2 and elemental Sb distributed throughout a matrix of InSb.

As was the case in the binary TlSb system, substrate temperature had little effect on the growth products produced. Throughout a range of temperatures from 250 - 425°C the surface morphology remained the same containing a two phase mixture of Tl_7Sb_2 and elemental Sb distributed throughout a matrix of InSb. Thus, the Tl_7Sb_2 phase seems to be the dominate phase in the ternary InTlSb system as was in the binary TlSb system.

Substrates of InP, InSb and GaSb with the (100) orientation had no effect on the growth products and produced only slight changes in the morphology. The InSb and GaSb substrates produced flatter two phase mixtures of Sb and Tl_7Sb_2 . It is believed that this is due to the Sb containing materials tendency to wet the antimonide substrates more easily but a factor for the differences in lattice parameter between InP and InSb or GaSb may need to be considered.

Adjusting the V/III ratio produced only slight changes in the morphology and no changes in the phases produced. Figure 5.7 (a), (b) and (c) are InTlSb samples grown under identical conditions with the exception of Tl cell temperature which was 515°C, 530°C and 545°C respectively. As one can see the morphology goes from InSb with no Tl to an immediate formation of the two phase mixture of Sb and Tl_7Sb_2 in an InSb matrix. As the Tl cell temperature is increased, the amount of Tl_7Sb_2 is increased. There were no samples produced that formed with excess Tl on the surface as long as a sufficient Sb flux

was supplied to the growth surface. Increasing or decreasing the Sb flux did not change the phases produced but only changed the amount of excess Sb in the two phase mixture or Ti_7Sb_2 and excess Sb.

Oxidation of the InTiSb system was identical to what was found in the TiSb system. The Ti_7Sb_2 phase begins to show signs of oxidation after exposure to air to periods greater than a few hours and will completely oxidize in over a month leaving only Ti_2O and Sb.

The attempts to cap the InTiSb system proved to be difficult once again. Figure 5.8 (a) and (b) are samples grown under identical conditions; a 1000Å InSb buffer layer, 60 minutes of In, Ti and Sb, and a substrate temperature of 375°C. However, Figure 5.8 (b) was capped with InSb for 20minutes (approximately 2000Å) at a substrate temperature of 300°C. It was hoped that the reduced substrate temperature employed during the growth of the cap would be able to suppress segregation and help bury the Ti_7Sb_2 phase. The only difference in morphology between these samples is the presence of small bar shaped growths that appear on the capped sample. These bars were found to contain pure Sb and are most likely a consequence of the increased sticking coefficient of Sb at the reduced substrate temperature. Although it is not evident in the secondary electron images of the surface, the average size of the two phase mixtures of Ti_7Sb_2 and Sb are increased. This would indicate that substrate temperature was low enough to prevent significant Ti desorption from the surface but still high enough to allow the Ti_7Sb_2 phase to coalesce during the cap layer formation. Superlattice structures of InSb/InTiSb were attempted at substrate temperatures as low as 300°C but were unsuccessful in burying the Ti_7Sb_2 phase.

5.5 Summary of the InTiSb Ternary Compounds

Incorporation of Ti in InSb produced a mixture of Ti_7Sb_2 and Sb in a matrix of InSb. The phases produced were virtually unaffected by changing the substrate material or

substrate temperature. Changing the V/III ratio only varied the amount of the Tl_7Sb_2 phase and/or the amount of excess Sb on the surface. The Tl_7Sb_2 phase was found to have a complicated multi-atom per lattice point, CsCl type structure. This Tl-rich phase was found not to oxidize as rapidly in air as the phase produced in the arsenide system but still will completely oxidize in approximately one month. The ability to cap or form a superlattice with the Tl_7Sb_2 phase was unsuccessful even at growth temperatures as low as 300°C .

5.6 Modification of Theory Based on Antimonide Experimental Data

The experimental work on the antimonide system presented here induced changes in the predicted structure of TlSb . The calculation of the cohesive energy for the Tl_7Sb_2 phase was not done until this experimental work showed it to be the dominant phase. Upon further calculations it was found that the CsCl Tl_7Sb_2 phase was more stable than the zincblende TlSb , CsCl TlSb , or the NaCl TlSb structures^{22,61}.

5.7 Segregation Theory Pertaining to the Tl Containing III-V Materials

Upon conclusion of a rigorous experimental program to determine the extent to which it is possible to incorporate Tl into normal III-V materials it is obvious that the process will be very difficult at best. It was found that Tl has a tendency for cationic behavior as reported previously in the chemical literature. This tendency increases with increasing molecular weight in the column III and column IV elements in the periodic table. The inherent problem that must be overcome is the inability of Tl to hybridize the $6s^2$ electron shell. Without hybridization of this $6s$ electron shell only the $6p^1$ electron participates in the bonding. Hence Tl is unable to participate in the normal covalent bonding that is needed for the formation of tetrahedrally coordinated III-V materials. This

reduced tendency for hybridization of the s electrons is referred to as the lone inert pair effect.

One potential method for overcoming this effect may be to chemically induce hybridization. One example of this approach is the successful incorporation of Sn from TESn versus elemental Sn. In this case the gaseous source, TESn, is tetrahedrally hybridized and has a much lower tendency for segregation at the growth surface. The elemental Sn which arrives in a metallic state segregates severely. Since the TESn is sp^3 hybridized, it is already been chemically forced in to a bonding state where the electrons in its outer most s and p shells participate in bonding. Thus it is easier for this chemically induced covalent state to incorporate without segregation.

Formation of a trivalent Tl precursor such as triethylthallium (TETl) or trimethylthallium (TMTl) may be the key to reducing the tendency of Tl to segregate. Hence making Tl incorporation a factor of solubility which is expected to be sufficient to produce 0.1 eV bandgaps in the arsenide and antimonide systems where only small amounts of Tl are needed. Unfortunately a tetrahedrally hybridized Tl source is not commercially available⁶². TETl has been reported in the literature, but is apparently quite unstable⁶³. Until such sources become available it is unlikely that Tl-containing compounds will become technologically feasible.

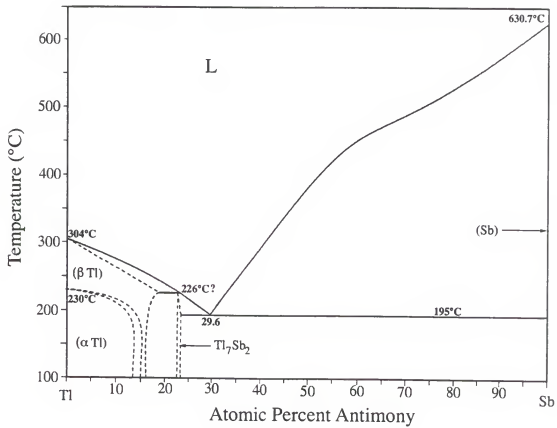
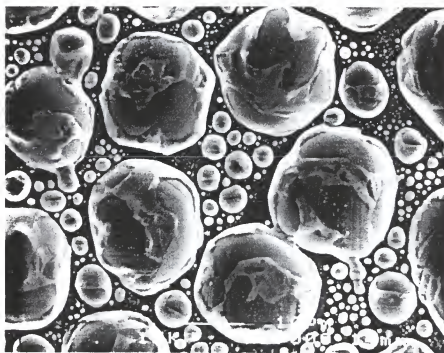


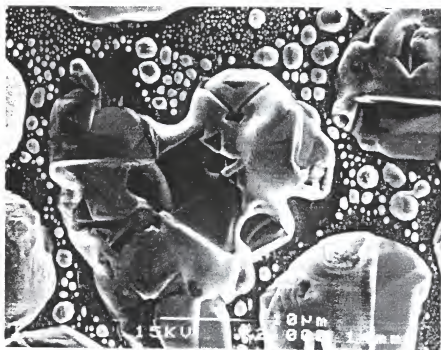
Figure 5.1: Phase diagram of the Tl-Sb binary system. Redrawn from reference (54).



Figure 5.2: Backscattered electron image of two phase mixture containing Tl_7Sb_2 and Sb. Light areas of contrast are Tl_7Sb_2 and darker areas are Sb. The background is the GaAs substrate.



(a)



(b)

Figure 5.3: Contrasting morphologies as seen by SEM in two-phase mixture of Sb and Tl_7Sb_2 as grown of (a) GaAs, (b) GaSb at 2,000x.

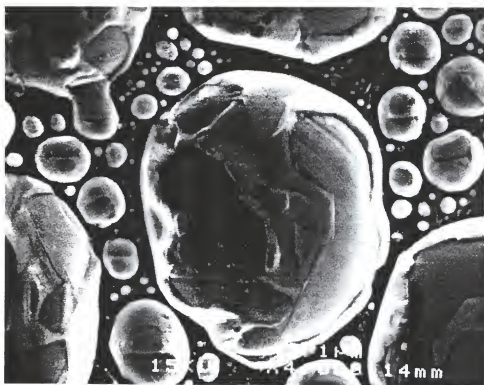
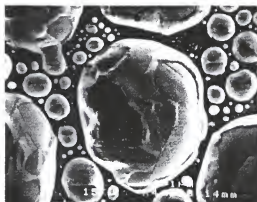


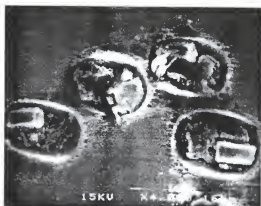
Figure 5.4: SEM image of the Tl_7Sb_2 and Sb two phase mixture illustrating the increased amount of Sb when the V/III ratio is increased.



(a)



(b)



(c)

Figure 5.5: Progression of oxidation in Tl_7Sb_2 phase; (a) as grown at 4,000x, (b) after two weeks in air at 10,000x, (c) after 1 month in air and HF dip etch to remove TiO_x at 4000x.

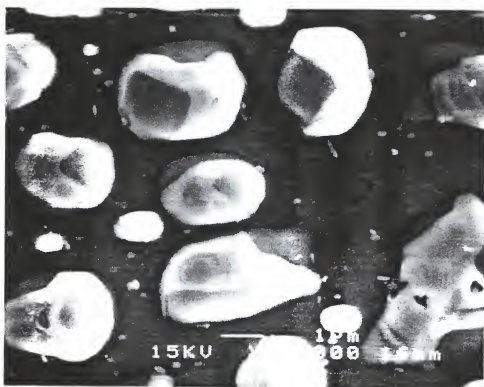
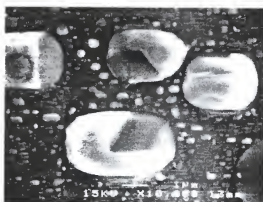


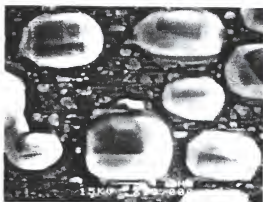
Figure 5.6: SEM image of a two phase mixture of Tl_7Sb_2 and Sb in a matrix of InSb formed using elemental Tl, Sb, and Tl at a substrate temperature of 275°C . Magnification is at 10,000x.



(a)

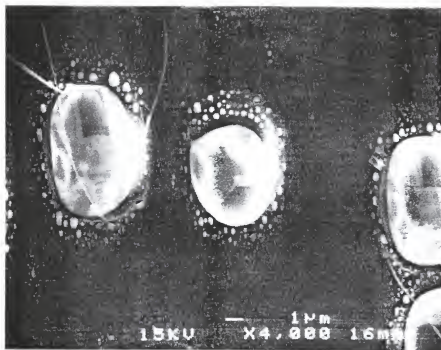


(b)

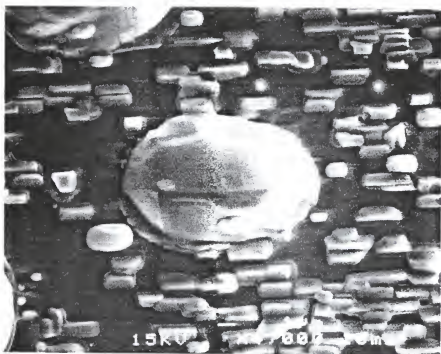


(c)

Figure 5.7: SEM images of InTiSb as TI cell temperature is increased from (a) 515°C magnification at 1,000X, (b) 530°C magnification at 10,000x and (c) 545°C magnification at 10,000x.



(a)



(b)

Figure 5.8: SEM images of InTISb sample morphology (a) without InSb cap and (b) with a 2000Å InSb cap grown at 300°C.

CHAPTER 6 N-TYPE DOPING OF III-V MATERIALS

6.1 Introduction

It is necessary to identify dopants, both n- and p-type, which can provide a wide range of carrier concentrations. These dopants must be thermally stable, have a low diffusivity and be able to attain abrupt doping junctions in order to be useful in the fabrication of devices. Furthermore, the dopants must have reasonable incorporation characteristics at very low growth temperatures, due to the desorption of Tl from the growth surface for substrate temperatures above 425°C as previously described.

S, Si, and Sn are the standard n-type dopants used in InP. These dopant sources are commercially available in a variety of alkyl and hydride forms. Unfortunately, problems with their usefulness, including many safety issues, still need to be addressed. Some of the current limitations of these sources include toxicity, controllability and thermal stability. For example, the more commonly used Si precursors, SiBr₄, and Si₂H₆, tend either to produce memory effects⁶⁴ or exhibit unacceptably low incorporation efficiencies⁶⁵. Clearly there is a need for alternative n-type dopants that are less toxic and incorporate efficiently even at low temperatures.

Tellurium doping of III-V materials has been reported in both metal organic vapor phase epitaxy (MOVPE)^{66,67}, and metal organic molecular beam epitaxy (MOMBE)⁶⁵, using the alkyl source diethyltellurium (DETe)^{65,67}. These reports include data showing good incorporation efficiency and the ability to achieve relatively high doping levels in GaAs and InP⁶⁵⁻⁶⁷. However, some problems were encountered. Clawson et al., for

example, found using Polaron profiling that the carrier concentration continually decreased toward the substrate. This suggested a problem with memory effects or possibly surface segregation. In addition Weyers et al. found that the incorporation efficiency was low in UHV growth due to the high thermal stability of the source molecule. It was suggested that less stable sources might be able to achieve the same doping concentrations with lower fluxes. This of course would also decrease the risk of memory effects.

One possible candidate for a less thermally stable source is diisopropyltellurium (DIPTe) however, the weak bonding in this source makes it too unstable to store and transport into the chamber. A novel method for improving its transportability is the formation of an adduct⁶⁸. This can be accomplished by taking two relatively unstable alkyl molecules like DIPTe and triisopropylindium (TIPIIn), and combining them to form a very stable adduct molecule. This adduct stabilized molecule can be seen in Figure 6.1. Coordinate covalent bonding retains the low decomposition temperature while improving the source stability over that typically found in the alkyls. Furthermore, this source is not as pyrophoric as the normal group III or group V alkyls and is not as toxic as the group VI hydrides like H_2S .

6.2 Incorporation Characteristics of TIPIIn-DIPTe

The decomposition behavior of the TIPIIn-DIPTe compound can be seen in Figure 6.2 where the electron and Te concentrations are plotted versus the TIPIIn-DIPTe flux. Through the range of dopant concentrations the incorporation is linear with TIPIIn-DIPTe flux. SIMS analysis showed no C, Si, or S incorporation above the background for the InP:Te grown using 1 sccm of PH_3 . Thus the measured electron concentrations are due solely to Te, suggesting that the activation at high Te fluxes is quite good. Linear behavior was also observed at a growth temperature of 425°C.

As one might expect given the size difference between Te and P, the incorporation of Te introduces a significant amount of strain into the material. This can be seen in Figure 6.3, where the in-plane lattice strain from the 004 direction is plotted as a function of increasing TIPIn-DIPTe flux. Both the FWHM and strain increase with increasing Te concentration. The amount of substitutional Te can be estimated from this data using Vegard's law. A comparison of this concentration with the SIMS suggests that virtually all of the incorporated Te is substitutional. This is in agreement with the good electrical activation observed in the electrical measurements.

In spite of the strain that has been introduced into the lattice, films with thicknesses up to 0.5 μm show no evidence of relaxation when examined by cross-sectional transmission electron microscopy (XTEM) and SEM. However, films grown at 525°C with Te concentrations of $1.0 \times 10^{20} \text{ cm}^{-3}$ show a rough surface due to the formation of surface pyramids as can be seen in Figure 6.4(a). By lowering the growth temperature to 475°C, these pyramids can be eliminated, as shown in Figure 6.4(b). These specular morphologies are maintained to temperatures as low as 375°C, Figure 6.4(c). Electrically the very heavily doped material with good morphology shows evidence of impurity banding at high Te concentrations as shown in the temperature dependent Hall data in Figure 6.5. Because of the very high doping level, the mobility is low, and may be limited by hopping conduction.

Since the Te sits on the group V site, one might expect that increasing the phosphine flow during growth would decrease the Te incorporation. This is in fact the case as can be seen in Figure 6.6 where the Te concentration as measured by SIMS decreases with increasing phosphine flow. At high PH_3 flows, carbon from the TEIn, present at a concentration of $\sim 1 \times 10^{19} \text{ cm}^{-3}$, dominates the electrical properties for moderately doped Te films. Thus, as is usually the case for InP, low V/III ratios reduce the background carbon concentration.

One of the reasons for investigating an adduct-type precursor is to enable the efficient incorporation of n-type dopants at low substrate growth temperatures. Due to the weak bonding in TIPIn-DIPTe, doping at low substrate growth temperatures can be achieved efficiently as seen in Figure 6.7, where the C and Te concentrations as determined by SIMS are plotted as a function of substrate growth temperature. The Te concentration only drops slightly with decreasing temperature, even at T_g as low as 375°C. At temperatures above 475°C the Te concentration also drops, presumably due to enhanced desorption. It should be noted that the carbon concentration increases as substrate growth temperature decreases; however, this is due to the incomplete pyrolysis of the triethylindium, not to the Te source, since the carbon background did not change significantly when the TIPIn-DIPTe was switched off or on. This unintentional doping can be eliminated by using elemental In rather than TEIn.

Though the decomposition behavior of the source seems well behaved, the incorporation of the resulting Te gives clear evidence of segregation. This can be seen in the SIMS profile shown in Figure 6.8, taken from a film grown using three different fluxes of Te at a growth temperature of 475°C. The two peaks furthest to the right were intended to be square profiles $\sim 2500\text{\AA}$ thick. Segregation has caused substantial smearing. The peak on the far left of the plot shows improved abruptness at the highest Te flux due to saturation of the dopant at the surface. The smearing of the profiles is not due to diffusion of the Te, as annealing at 850°C for 1 minute of the same sample as shown in Figure 6.8 produced virtually no change in the SIMS profiles. Thus, segregation clearly is the problem.

As expected, this segregation of the Te can be suppressed by decreasing the substrate growth temperature, as shown in the SIMS analysis in Figure 6.9. All Te doping profiles were accomplished by using the same Te flux at various growth temperatures. The two peaks on the right of the figure show profiles with abrupt turn-on and turn-off. The peak on the left hand side of the figure grown at 525°C shows a less abrupt turn-on and a

very poor turn off. In addition to reduced temperature, increasing the V/III ratio was found to suppress segregation as well. However, as discussed previously the C background at large PH_3 flows becomes extremely high and dominates the electrical properties.

6.3 Thermal Stability of Te Doped InP

For many device technologies, improved performance mandates the use of increasingly higher doping levels. In InP-based heterojunction bipolar transistors (HBT), for example, InP can be employed rather than InGaAs. However, InP is generally more difficult to dope to high concentrations than InGaAs. Because of their reduced tendency to incorporate amphotERICALLY, group VI donors are expected to produce the highest uncompensated electron concentrations. For these reasons, Te has been investigated as a potential n-type dopant for InP^{65-67,69-71}. Earlier in this chapter we have shown that triisopropylindium-di-isopropyltellurium can be used to achieve doping concentrations as high as $1.4 \times 10^{20} \text{ cm}^{-3}$ over a wide range of growth temperatures⁶⁹.

Before doping from TIPIn-DIPTe can be employed, the thermal stability of Te-doped material must be examined. Doping from diethyltellurium (DETe) has been studied using both MOMBE⁶⁵ and MOCVD^{66,67,70} however there have been no reports of the stability of Te during post-growth thermal treatments. In order for Te to be used in device structures, it must be demonstrated that the electrical properties of the Te doped layers can withstand such conditions. Hence, the structural and electrical stability of Te-doped InP was investigated.

The proximity capping method was used to maintain the epilayer surface during annealing. Surface morphologies remained specular up to annealing temperatures of 800°C. At temperatures above 850°C, however, the InP layer begins to degrade from the loss of P from the surface. This can be seen by the appearance of In droplets on the surface in Figure 6.10. Surface morphologies in these samples could be very different

depending on what growth temperature was used. This was found to be from surface segregation where the Te accumulates at the surface at temperatures above 475°C and leads to the formation of hillocks shown and discussed previously in Figure 6.4(a). For samples grown at or below 475°C, such segregation does not occur. In these cases the electrical activity of the incorporated dopant is roughly 100% as determined from a comparison of Hall measurements and SIMS analysis. The absence of hillocks in the annealed material suggests that once the Te is incorporated into a substitutional site, it remains fairly immobile. This can be seen in Figure 6.11 where the peak concentration of Te and the Te profile remain virtually identical before and after annealing at temperatures as high as 850°C.

While the surface morphologies are relatively insensitive to annealing up to 800°C, the electrical properties begin to degrade at lower temperatures. Figure 6.12 shows the effect of increasing annealing temperature on the carrier concentration and mobility as determined by hall measurements. Annealing at 650°C appears to increase the carrier concentration slightly which also reduces the mobility. Annealing at higher temperatures results in a continual decrease in the electron concentration. Above 700°C, this decrease results in a corresponding increase in mobility. Similar behavior has been observed for heavily carbon doped GaAs,⁷²⁻⁷⁴ and is usually attributed to the formation of dopant clusters.

The decrease in carrier concentration is accompanied by a decrease in the strain observed in the layer as shown in Figure 6.13. The initial strain is due to the size difference between Te and P. As for carrier concentration, low ($\leq 650^\circ\text{C}$) annealing temperatures do not affect the strain. For temperatures greater than 650°C, epilayer strain decreases with increasing temperature. The decrease in strain could be caused by a number of factors including the formation of strain relieving defects such as dislocations in the epilayer or the epilayer-substrate interface, diffusion of Te, or a decrease in the concentration of substitutional Te atoms. It is unlikely that dislocation generation is

responsible for the strain reduction since neither SEM nor TEM show any evidence of dislocation propagation. Out-diffusion of Te can also be eliminated since SIMS analysis does not indicate a redistribution of the Te profile.

Given the absence of diffusion, it is most likely that the decrease in stain observed upon annealing is due to the formation of Te clusters. Such a mechanism would also account for the reduction in the electrical activity and increase in carrier mobility obtained with annealing. Attempts to prove the existence of the Te clusters by both XTEM and RBS-C were unsuccessful, indicating the small size of the Te clusters. Given the low diffusivity measured for Te in InP, small size clusters would be expected since larger clusters would require a much longer diffusion distance to form. Similar behavior in heavily carbon doped GaAs has been attributed to the formation of carbon-carbon pairs on the As sub-lattice⁷²⁻⁷⁴. While a similar configuration for Te seems unlikely due to the size of the Te atom, it is possible that pairing may be occurring in interstitial sites. Further investigation is needed to clarify the exact location of the nonelectrically active Te.

6.4 Conclusions

Trisopropylindium-diisopropyltellurium was found to give clean, efficient decomposition, even at low substrate growth temperatures without increasing the background C concentration. Electron concentrations as high as $1.4 \times 10^{20} \text{ cm}^{-3}$ were obtained with excellent electrical activation and specular morphology in layers grown at $T_g \leq 475^\circ\text{C}$. Although a severe surface segregation problem was observed, it was shown that it could be controlled by either increasing the V/III ratio or decreasing the substrate growth temperature over the range $475 - 375^\circ\text{C}$. The thermal stability and diffusion characteristics of heavily doped InP:Te layers were examined. SIMS analysis shows little change in the dopant profile or the peak concentration of Te, indicating little or no diffusion over the temperature range ($500 - 850^\circ\text{C}$) studied. However, it was determined that both

the electron concentration and epilayer strain decrease with increasing annealing temperature for temperatures above 650°C. This suggests the formation of Te clusters though XTEM and RBS-C could not reveal any evidence of Te precipitation. Below ~700°C, the InP:Te layers were stable with respect to temperature.

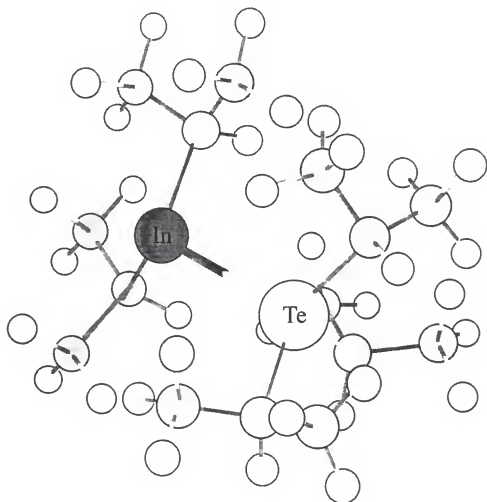


Figure 6.1: Molecular structure of the adduct stabilized Te precursor, triisopropylindium-diisopropyltellurium, $[(\text{CH}_3)_2\text{CH}]_3\text{InTe}[(\text{CH}_3)_2\text{CH}]_2$. Tellurium and In are as labeled, carbon are represented as gray and hydrogen as white.

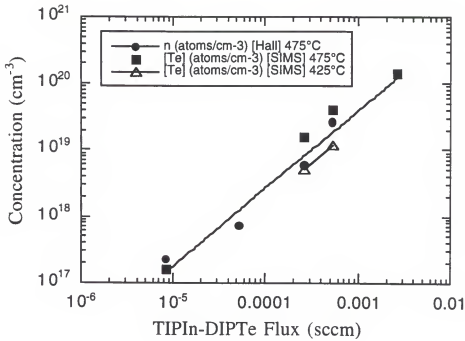


Figure 6.2: Concentration of atoms as measured by Hall and SIMS for the various TIPIIn-DIPTe fluxes. Samples were grown using TEIn and 1 sccm of PH_3 .

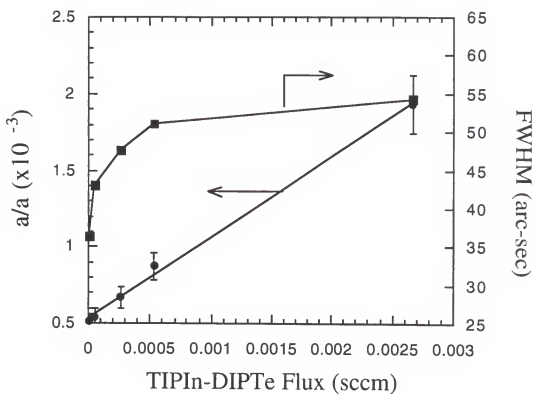
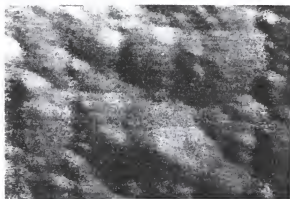


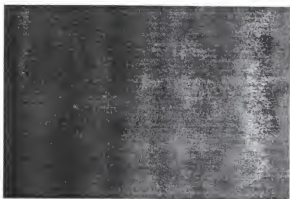
Figure 6.3: In plane lattice strain in the 004 direction as a function of TIPIIn-DIPTe flux as determined by high-resolution x-ray diffraction.



(a)



(b)



(c)

Figure 6.4: SEM images of the surface morphology at 4000X for (a) InP:Te $T_g=525^\circ\text{C}$, $n[\text{Te}]=1.0 \times 10^{20} \text{ cm}^{-3}$, (b) InP:Te $T_g=425^\circ\text{C}$, $n[\text{Te}]=1.4 \times 10^{20} \text{ cm}^{-3}$, (c) InP:Te $T_g=375^\circ\text{C}$, $n[\text{Te}]=1.4 \times 10^{20} \text{ cm}^{-3}$.

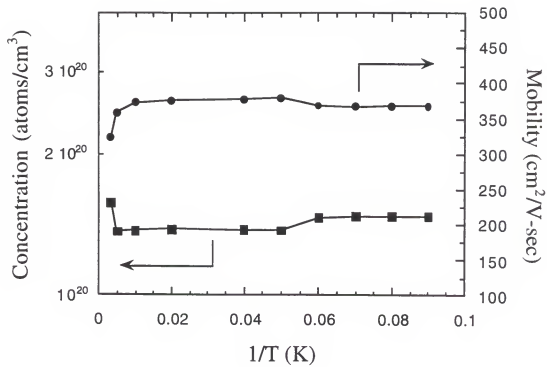


Figure 6.5: Temperature dependent Hall data for InP:Te.

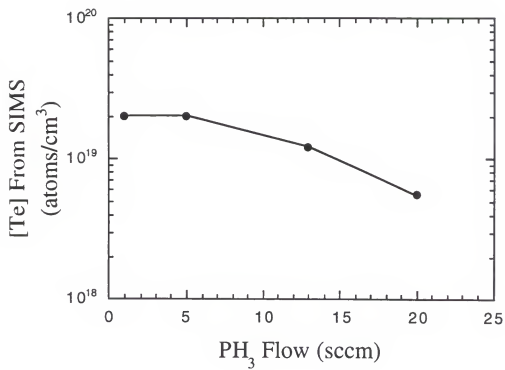


Figure 6.6: Concentration of Te atoms from SIMS, as a function of PH_3 flow.

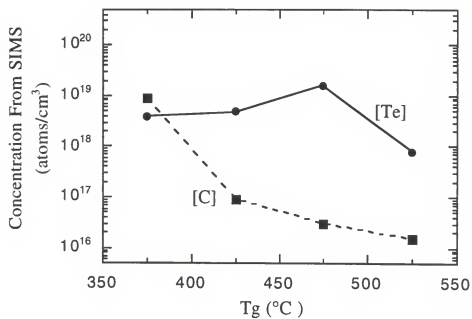


Figure 6.7: Concentration of Te and C atoms from SIMS as a function of T_g . Samples were grown using 1 sccm of PH_3 .

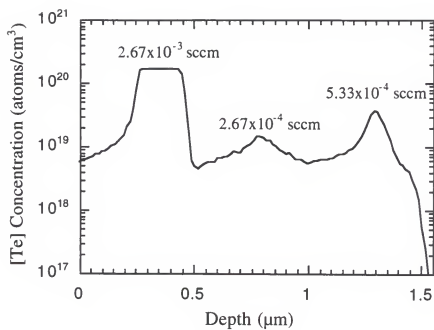


Figure 6.8: SIMS profile of the Te concentration as a function of depth through three different TIPIIn-DIPTe fluxes. ($T_g=475^\circ\text{C}$).

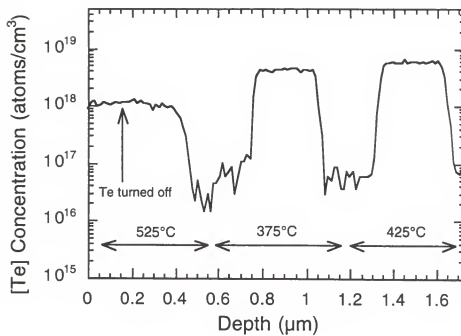


Figure 6.9: SIMS profile of Te concentration as a function of depth through three different substrate growth temperatures.

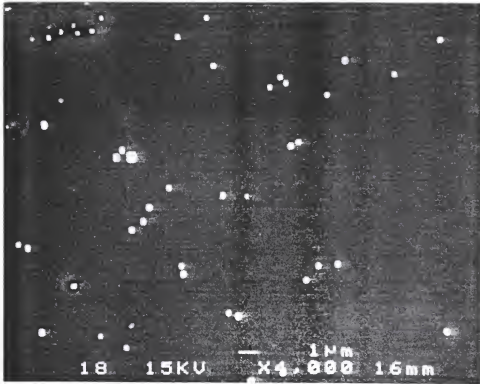


Figure 6.10: SEM surface micrographs of Te-doped InP grown at 475°C to a carrier concentration of $1.4 \times 10^{20} \text{ cm}^{-3}$ and annealed at 850°C for one minute using the proximity capping method in an RTA. White spots show evidence of In droplet formation due to the loss of P from the surface.

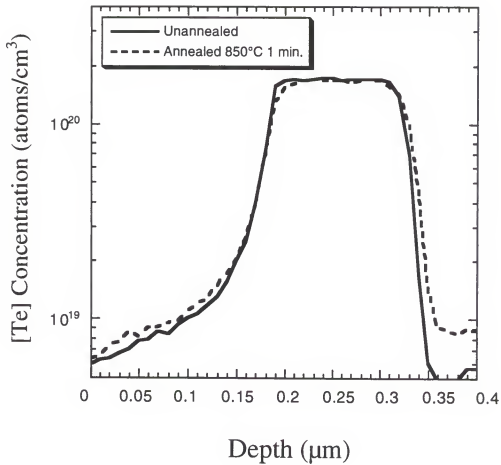


Figure 6.11: Te profiles as determined by SIMS before (solid line) and after (dashed line) annealing at 850°C.

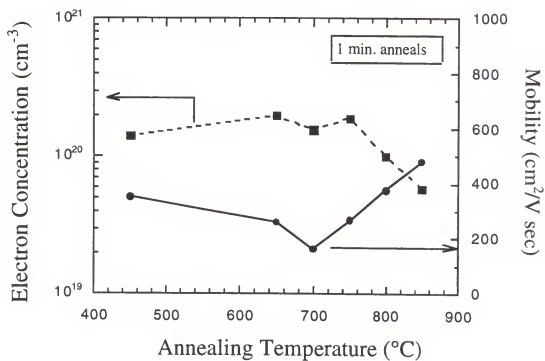


Figure 6.12: Room temperature electron concentration and mobility vs. annealing temperature for Te-doped InP. Annealing time was one minute.

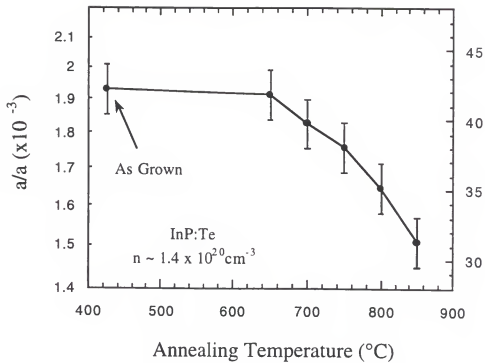


Figure 6.13: In plane lattice strain in the 004 direction as a function of annealing temperature. Annealing time was one minute.

CHAPTER 7 P-TYPE DOPING OF III-V MATERIALS

7.1 Introduction

While carbon has been proven to be an excellent p-type dopant for III-V materials containing gallium, it behaves as a highly compensated donor in InP⁷⁵. Although Be, Cd, Mg, and Zn have been used as acceptor dopants, each has drawbacks. The use of diethylberyllium (DEBe) as a gaseous dopant is discouraged due to the extreme toxicity of Be. Zn is most commonly used p-type dopant and can provide hole concentrations up to 10^{18}cm^{-3} in InP, though severe diffusion during growth and subsequent processing limits its usefulness. In addition the decomposition of diethylzinc (DEZn) is poor at low temperatures making it unsuitable for an effective p-type dopant of the Tl containing alloys. Similar levels of doping can be achieved using Mg. Moreover, the diffusion of Mg through the layer is much slower than Zn in III-V materials which makes it the preferred p-type dopant. Unfortunately, a severe reactor memory effect is encountered when Cp_2Mg or $(\text{MeCp})_2\text{Mg}$ are used as p-type precursors in MOCVD. Hence, abrupt changes in dopant profiles are virtually impossible without long periods of interrupted growth. This tailing effect has been attributed to strong interactions of the Mg precursors with the walls of the reactor⁷⁶ as well as the stainless steel inlet connectors in MOCVD systems⁷⁷. The memory effect is less of a problem in a lower pressure MOMBE-GSMBE system and abrupt junctions can be achieved using Cp_2Mg ⁷². Unfortunately, the lack of saturation in

this precursor often causes a delay in the turn-on of the dopant during growth making reproducibility in sophisticated devices a problem.

Bis-3-dimethylaminopropylmagnesium, Figure 7.1, has been proposed as an alternative p-type Mg dopant in an attempt to alleviate some of the aforementioned problems with the Cp_2Mg ⁶². By coordinately saturating the Mg p orbitals the Mg will become less electrophilic, making it less oxygen sensitive. Thus this precursor is less likely to undergo parasitic reactions with group V precursors and is less likely to adsorb on gas lines and injectors. Initial studies on the vapor pressure have shown it should be sufficiently volatile for MOMBE-GSMBE applications⁶³. However, initial growth studies found that this dopant source was too unstable, reacting with itself to form Mg clusters in the films. Clearly another p-type dopant was needed for the TI-containing materials and other low growth temperature doping applications.

In other III-V material systems, like GaAs, it was found that significant carbon, and hole, concentrations could be introduced through the use of halogenated methanes like CCl_4 or CBr_4 . CBr_4 in particular, shown in Figure 7.2, has been shown to produce significant improvement in efficiency relative to TMG and CCl_4 by factors of 750 and 150 respectively^{78,79}. The good electrical activity, high solubility and remarkably low tendency for diffusion have led to its extensive use for fabrication of a number of device structures requiring p-GaAs. Another area where the halocarbons have been particularly successful is in the doping of In-containing compounds such as InGaAs and InGaP. For example, a number of groups have now reported doping levels in excess of 10^{20} cm^{-3} in $\text{In}_{0.5}\text{Ga}_{0.5}\text{As}$ using either CCl_4 or CBr_4 ⁸⁰. This chapter will present the first study of carbon doping in InSb using CBr_4 .

7.2 Incorporation Characteristics of Carbon Tetrabromide

It was found that p-type InSb could be obtained quite easily from CBr_4 . As shown in Figure 7.3, the hole concentrations increases almost linearly with dopant flux until a maximum concentrations of $4.5 \times 10^{20} \text{ cm}^{-3}$ is achieved. This is the highest hole concentration yet reported for InSb using any dopant. The mobilities obtained in these films are comparable to those reported for other dopants. At the higher doping levels, the mobility decreases as expected. As the CBr_4 flux is increased to the highest fluxes, the carrier concentration begins to drop as well. This is believed to be due to the formation of carbon complexes other than $[\text{C}]_{\text{As}}$. High CBr_4 fluxes produce very poor epilayer morphology. The cause of this poor structural quality may be either parasitic etching or carbon has exceeded the solubility limit for this material. This poor structural quality is most likely the reason for the lack of electrical activity at the high dopant fluxes. Since no metal organics or hydrides were used for the growth of these InSb epilayers, no hydrogen contamination was expected. SIMS analysis of the epitaxial layers in fact showed no incorporation of either hydrogen or oxygen above the background.

As the amount of carbon is increased one might expect that the addition of a smaller atom substitutionally into the lattice would decrease the epilayer mismatch. This is the case as can be seen in Figure 7.4 which illustrates the change in lattice dimensions in the 004 direction as a function of CBr_4 flux. It should be noted that the critical thickness of an InSb film on an InP substrate is small in comparison to the layer thickness for the InSb:C samples. Hence, the InSb and InSb:C samples are assumed to be at least partially relaxed.

Figure 7.5 illustrates the morphology of the InSb films as seen by secondary electron imaging throughout a range of doping concentrations. As can be seen in Figure 7.5 (a), an undoped InSb film, the morphology is smooth and featureless showing no evidence of islanding growth or cross-hatching. Figure 7.5 (b) is a sample doped to a carbon concentration of $6.67 \times 10^{19} \text{ cm}^{-3}$. This sample also has a specular morphology and

no evidence of cross-hatching could be found. Finally, Figure 7.5 (c) shows the morphology obtained when growth of InSb is attempted while using a very high CBr_4 flux (~ 0.5 sccm). This sample is very rough and is believed to be polycrystalline.

The growth rate was found to be a function of growth temperature, as shown in Figure 7.6. The growth rate is believed to be changing due to the influence of the effective V/III ratio at the growth surface. In fact the dependence of growth rate on growth temperature is very similar to that observed with Sb cell temperature. At high Sb fluxes, the growth rate is suppressed, presumably due to enhanced desorption of the In from the growth surface due to site blocking by the Sb. It is likely that as the growth temperature is reduced the amount of Sb desorbing from the growth surface is also reduced, again resulting in site blocking by the Sb and a reduced sticking coefficient for the In. It is not yet known what effect, if any, altering the temperature or Sb flux will have on the flux dependence of the growth rate.

Similar to what has been reported for CBr_4 doping of other III/V materials, changing the growth temperature does not substantially alter the hole concentration, as shown in Figure 7.7, for temperatures below 450°C . At 450°C , the surface becomes In-rich, as evidenced by metal droplets at the surface. If the Sb cell temperature is increased to accommodate the enhanced loss of Sb from the surface at the elevated temperature, the hole concentration attained is similar to those observed at lower temperatures. Similarly, the mobility does not appear to be a strong function of growth temperature, returning to the average value when the Sb flux is increased at 450°C . These results show that like GaAs, the electrical properties are relatively independent of growth temperature when growing under Group V rich conditions.

Growth rates between 80 and $160 \text{ \AA}/\text{min}$. were obtained for all of the InSb:C samples. Growth rate of the InSb epilayers was found to be dependent on CBr_4 flow. Figure 7.8 shows the growth rate dependence of the epilayers on CBr_4 flow rate. All samples in this figure were grown at 400°C . There is some evidence of parasitic etching

due to the release of Br at the growth surface. Similar behavior has also been observed in GaAs.

7.3 The Behavior of C in III-V Materials

In most Ga-containing III-V materials, like GaAs or p-AlGaAs, carbon has proven to be almost exclusively an acceptor. By contrast, carbon doping of In-containing binaries such as InP has only been found to produce compensated n-type material. Ternary alloys of these materials, such as $\text{In}_x\text{Ga}_{1-x}\text{As}$, can exhibit either type depending upon the growth conditions used. In this study we have shown that InSb does not follow the behavior exhibited by InP. To first order this behavior can be explained by the relative strengths of the group III-carbon bond and the group V-carbon bond. The Ga-C bond is significantly stronger than both the As-C and In-C bonds. As a result, there exists a thermodynamic driving force for the incorporation of C acceptors in GaAs, as reflected in the very high hole concentrations observed in this material, as shown in Figure 7.9. InP, by contrast, exhibits the opposite behavior, producing material which is slightly compensated n-type^{13,81}. In general as the molecular weight of the species is decreased, it forms a stronger bond with carbon, making the net bond energy difference, $E_{\text{III-C}} - E_{\text{V-C}}$ lower and reducing the driving force for incorporation of carbon acceptors. This argument explains the maximum carrier concentration observed in the III-V materials which have been studied to date. It should be noted, however, that all of the maximum levels reported thus far have been attained in ultrahigh vacuum (UHV), where growth conditions can be made most favorable for incorporation of carbon. Using this model it is expected that carbon will behave as an acceptor in InSb. However, based upon the trends shown in Figure 7.9, it is doubtful that the same ultra high doping levels that have been observed in GaAs and InSb could ever be replicated in InAs. Thus it appears that carbon is a suitable acceptor for InSb but not for InAs, even under the favorable growth conditions found in UHV.

Further predictions from this model can be applied to the behavior of C in the Tl-containing materials. In all Tl binary cases (TlP, TlAs and TlSb), carbon is predicted to act as a donor based on their respective C-III and C-V bond strengths. Similarly, the addition of carbon into the ternary InTlP and InTlAs systems is also expected to behave as a donor. However, for moderate concentrations of Tl in InTlSb (including those needed to achieve a 0.1 eV bandgap) carbon is expected to be an acceptor. Hence with its low temperature efficiency, a suitable p-type dopant for the most promising of the Tl containing III-V material systems.

7.4 Conclusions

For InSb, hole concentrations up to $\text{mid-}10^{20} \text{ cm}^{-3}$ were obtained at growth temperatures up to 450°C . This is believed to be the highest hole concentration yet reported for p-InSb. The hole concentration was found to be dependent on dopant flux and V/III ratio but not on growth temperature. A model for predicting the behavior of C in III-V materials was presented based on the strength of the C-III and C-V bond strengths predicting carbon to be an acceptor in InSb which was confirmed in this chapter.

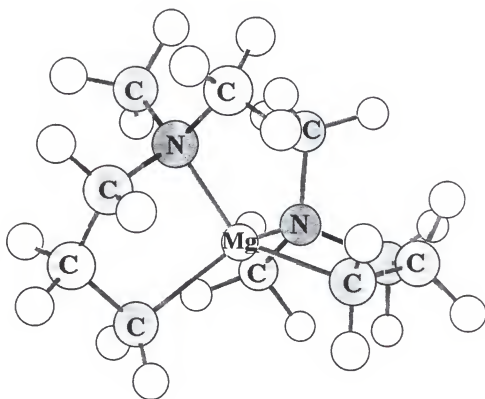


Figure 7.1: Structure of the intramolecularly saturated Mg compound bis-3-(dimethylamino)propylmagnesium molecule $[(\text{CH}_3)_2\text{N}(\text{CH}_2)_3]_2\text{Mg}$.

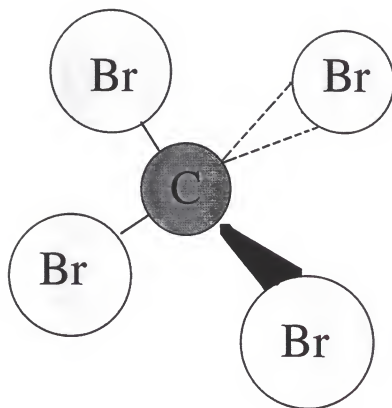


Figure 7.2: Molecular structure of carbon-tetrabromide CBr_4 .

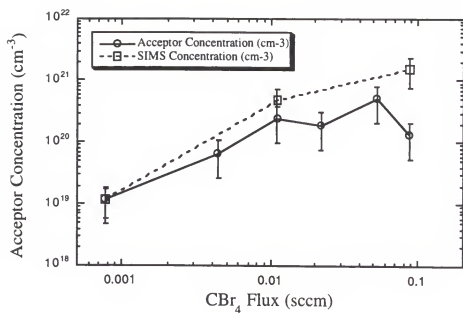


Figure 7.3: Concentration of atoms as measured by Hall and SIMS for various CBr_4 fluxes. Samples were grown using elemental In at a substrate temperature of 400°C .

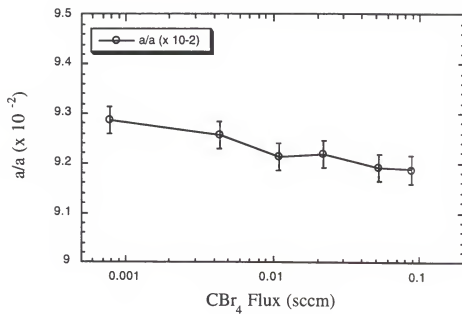
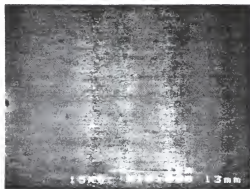


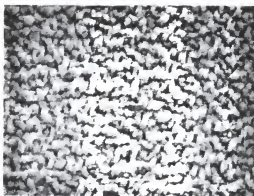
Figure 7.4: In plane lattice strain in the 004 direction as a function of CBr₄ flux as determined by high-resolution x-ray diffraction.



(a)



(b)



(c)

Figure 7.5: SEM micrographs showing the morphology of InSb epilayers grown on InP at 400°C, (a) undoped, (b) moderately doped with CBr_4 to an acceptor concentration of $6.67 \times 10^{19} \text{ cm}^{-3}$, and (c) heavily doped with CBr_4 to an acceptor concentration of $1.89 \times 10^{20} \text{ cm}^{-3}$.

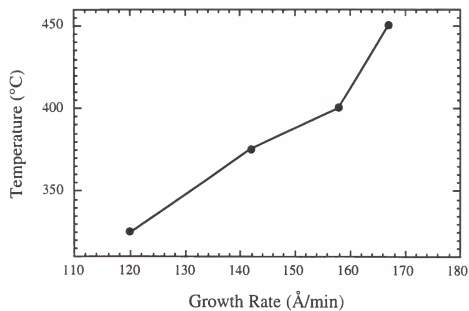


Figure 7.6: Relationship between growth rate and growth temperature.

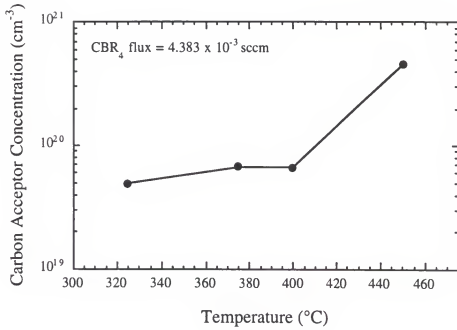


Figure 7.7: Variation of hole concentration with growth temperature.

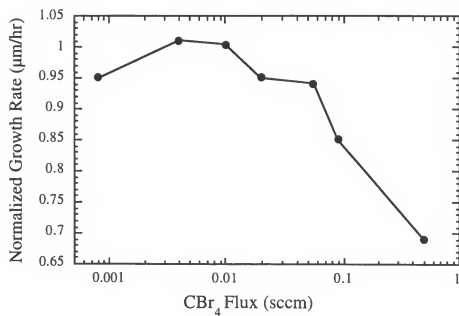


Figure 7.8: Dependence of growth rate on CBr_4 flux for InSb grown at 400°C .

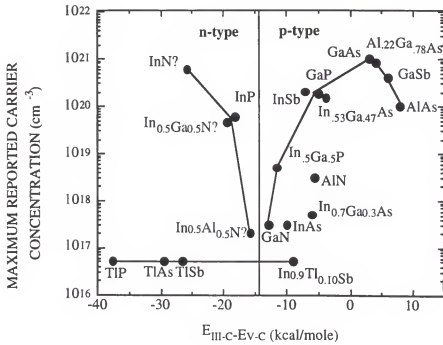


Figure 7.9: Maximum reported carrier concentration for materials with various group III-carbon and group V-carbon bond strengths as a function of the difference between the two bond strengths. Data taken from : InP¹³, GaP⁷⁸, InGaP⁸², InGaAs⁸⁰, GaAs⁸³, GaSb⁸⁴, AlAs⁸⁵, AlN⁸⁶, GaN⁸⁷, InAs⁸⁸, InN⁸⁹ and InGaN⁸⁹. Value for InSb obtained in this study. Ti binary compounds shown for comparison.

CHAPTER 8 CONCLUSIONS AND FUTURE RECOMENDATIONS

8.1 Conclusions

The growth, doping and characterization of the Tl- and InTl-containing material systems have been attempted using gas-source molecular beam epitaxy (GSMBE) using a combination of elemental group III sources and elemental and precracked gaseous group V sources. Tl was found to incorporate to an atomic fraction $<1\%$ in the phosphide system while some higher Tl-content phases were obtained in the arsenide and antimonide systems. The arsenide system produced a Tl-As phase with an approximate ratio of 7:2, but only in the presence of excess elemental Tl and in an InAs matrix. Under some growth conditions, a ternary InTlAs phase was formed but only in the presence of both InAs and elemental Tl. The antimonide system produced a Tl-Sb phase with a ratio of 7:2 but only in the presence of excess Sb. A ternary InTlSb phase could not be produced, rather a combination of the Tl_7Sb_2 phase and InSb was created.

These phases were characterized by x-ray diffraction, electron microprobe, scanning electron microscopy, secondary ion mass spectrometry and Auger electron spectroscopy. The Tl sticking coefficient was found to depend heavily on the substrate growth temperature. For substrate growth temperature above 425°C the sticking coefficient of Tl is essentially zero. Both pure Tl and all the Tl-containing phases produced by GSMBE were found to oxidize readily in air. Precautions were taken to minimize exposure of these Tl-containing phases to air so that the characterizational results would remain unambiguous.

A model for the incorporation characteristics of Tl in III-V materials was proposed to explain segregation effects. This model is based on the tendency for cationic behavior in Tl. It is believed that this behavior reduces the tendency for higher molecular weight elements to hybridize the outer most s electrons. Hence, higher molecular weight elements such as Tl cannot attain the sp^3 bonding configuration needed for tetrahedral covalent bonding.

The novel dopant source triisopropylindium-diisopropyltellurium was studied as an n-type dopant in InP. Triisopropylindium-diisopropyltellurium was found to decompose at the low growth temperatures dictated by the sticking coefficient of Tl ($<425^\circ\text{C}$). Record n-type doping concentrations up to $1.4 \times 10^{20} \text{ cm}^{-3}$ with good electrical activation and specular morphologies were obtained in InP. The Te activation was found to be thermally stable up to a temperature of 675°C and dopant diffusion was not observed for anneals as high as 850°C for 1 minute.

The intramolecularly saturated Mg compound, bis-3-dimethylamino-propylmagnesium, was found to form Mg clusters making it unsuitable as a p-type dopant in III-V materials. However, carbon tetrabromide was found to produce record p-type doping concentrations in InSb. Acceptor concentrations as high as $5.6 \times 10^{20} \text{ cm}^{-3}$ were produced. A model for the behavior of carbon in III-V semiconductors was formed based on the relative bond strength of C-III and C-V bonds. The behavior of carbon was found to be linked to a thermodynamic driving force. As the $E_{\text{III-C}} - E_{\text{V-C}}$ strength increases, the tendency for carbon to sit on a group V site increases thereby making carbon behave as an acceptor. The Tl-C bond is relatively weak thus, using this model, carbon is predicted to behave as a donor for TIP, TIAs, TlSb and all compositions of InTIP and InTIAs. However, carbon is expected to be an acceptor in InTlSb for low concentrations of Tl.

A model summarizing these results can be found in Table 8.1. This table reviews the objectives of this research and states the corresponding results obtained.

Table 8.1: Objectives of this research and the corresponding results obtained summarizing the body of this work.

Evaluate feasibility of synthesizing Tl-V and In-Tl-V compounds by GSMBE.	Found that zincblende TlV and InTlV could not be formed under any growth conditions.
Determine electronic and structural properties of the TlV and InTlV materials.	Single phase material could not be produced hence, electronic properties are ambiguous. Some structural properties of the two phase systems identified.
Provide feedback to SRI model predicting the electronic and structural properties of the TlV and InTlV materials.	Provided feedback to SRI for model refinement including Tl_3Sb_2 phase stability as well as two phase mixtures in the antimonide and arsenide systems.
Evaluated potential dopant sources, both n- and p-type, for low temperature growth of InSb and the low temperatures thought to be needed to form TlV and InTlV.	Found suitable n- and p-type dopants for low growth temperature applications. Produced record n-type doping concentration in InP and record p-type doping in InSb.
	Additional findings: Proposed model to explain the behavior of carbon in III-V materials.
	Proposed model to explain the incorporation behavior of Tl in TlV and InTlV compounds.

8.2 Future Recommendations

Throughout this research it was found that the majority of problems encountered with Tl incorporation could be traced back to an unfavorable bonding environment. A model was proposed in Chapter 5 detailing the reasons why this occurs. To summarize, Tl has difficulty in the hybridization of the outer most s electrons and hence cannot attain the sp^3 bonding configuration needed to produce tetrahedral covalent bonding. It is likely that a trivalent source of Tl such as $TlCl_3$ is needed to chemically force Tl into the sp^3 bonding configuration. This is the only approach which appears to have any chance of producing TlV and $InTlV$ without a high group V over-pressure environment.

LIST OF REFERENCES

- (1) P. W. Kruse In Semiconductors and Semi Metals; R. K. Willardson and A. C. Beer, Eds.; Academic Press: New York, 1981; Vol. 18.
- (2) Y. Kanai; K. Shohno, Japanese Journal of Applied Physics, 1, 239, **1962**.
- (3) G. C. Osbourn; L. R. Dawson; R. M. Biefeld; T. E. Zipperian; I. J. Fritz; B. L. Doyle, Journal of Vacuum Science and Technology, A5, 3150, **1987**.
- (4) D. Long In Energy Bands in Semiconductors; John Wiley & Sons: New York, 1968.
- (5) R. F. C. Farrow; G. R. Jones; G. M. Williams; P. N. Sullivan; J. J. O. Boyle; J. J. M. Wotherspoon, Journal of Physics D, 12, L117, **1979**.
- (6) J. M. Kuo; S. S. Pei; S. Hui; S. D. Gunapala; B. J. Levine, Journal of Vacuum Science and Technology, B10, 995, **1992**.
- (7) B. J. Levine; C. G. Bethea; K. G. Glogousky; J. W. Stayt; R. E. Leibenguth, Semiconductor Science and Technology, 6, C114, **1991**.
- (8) K. Y. Ma; Z. M. Fang; R. M. Cohen; G. B. Stringfellow, Journal of Applied Physics, 70, 3940, **1991**.
- (9) A. M. Jean-Louis; C. Hamon, Physica Status Solidi, 34, 341, **1969**.
- (10) A. M. Jean-Louis; B. Ayrault; J. Vargas, Physica Status Solidi, 34, 329, **1969**.
- (11) K. T. Huang; C. T. Chiu; R. M. Cohen; G. B. Stringfellow, Journal of Applied Physics, 75, 2857, **1994**.
- (12) J. L. Zilko; J. E. Greene, Journal of Applied Physics, 51, 1549, **1979**.
- (13) J. H. Oh; F. Fukuchi; H. -C. Kang; M. Konagai, Journal of Crystal Growth, 164, 425, **1996**.
- (14) A. J. Noreika; W. J. Takei; M. H. Francombe; C. E. C. Wood, Journal of Applied Physics, 53, 4932, **1982**.
- (15) M. van Schilfgaarde; A. -B. Chen; S. Krishnamurthy; A. Sher, Applied Physics Letters, 62, 1857, **1993**.
- (16) M. van Schilfgaarde; A. -B. Chen; S. Krishnamurthy; A. Sher, Applied Physics Letters, 65, 21, **1994**.

- (17) S. Iyer; S. Chowdhury-Nagle; J. Li; K. K. Bajaj, Presented at Spring Meeting of the Materials Research Society, San Francisco, CA, 1996.
- (18) Y. H. Choi; C. Besikci; R. Sudharsanan; M. Razeghi, *Applied Physics Letters*, **63**, 361, **1993**.
- (19) M. Razeghi; J. D. Kim; S. J. Park; Y. H. Choi; D. Wu; E. Michel; J. Xu; E. Bigan, *Institute of Physics Conference Series*, **145**, 1085, **1996**.
- (20) A. -B. Chen; A. Sher In *Semiconductor Alloys*; Plenum Press: New York, 1995.
- (21) M. Berding, unpublished 1997.
- (22) M. A. Berding; M. van Schilfgaarde; A. Sher, unpublished 1996.
- (23) M. van Schilfgaarde; M. Berding, *Bulletin of the American Physical Society*, **39**, 393, **1994**.
- (24) A. -B. Chen; M. van Schilfgaarde; A. Sher, *Journal of Electronic Materials*, **22**, 848, **1993**.
- (25) C. E. C. Wood; A. Noreika; M. Francombe, *Journal of Applied Physics*, **59**, 3610, **1986**.
- (26) Y. H. Choi; P. T. Staveteig; E. Bigan; M. Razeghi, *Journal of Applied Physics*, **75**, 3196, **1994**.
- (27) P. T. Staveteig; Y. H. Choi; G. Labeyrie; E. Bigan; M. Razeghi, *Applied Physics Letters*, **64**, 460, **1994**.
- (28) C. R. Abernathy, unpublished 1997.
- (29) R. Stokhuyzen; C. Chieh; W. Pearson, *Canadian Journal of Chemistry*, **55**, 1120, **1977**.
- (30) G. Moh, *Neues Jahrb. Mineral*, **144**, 291, **1982**.
- (31) *Chemistry of Aluminium, Gallium, Indium and Thallium*; A. J. Downs, Ed.; Blackie A&P: 1993.
- (32) C. R. Abernathy, *Materials Science and Engineering R*, **14**, 203, **1994**.
- (33) M. B. Panish In *Gas Source Molecular Beam Epitaxy*; Springer-Verlag: 1993.
- (34) C. J. Santana, Ph. D. Dissertation, University of Florida, 1996.
- (35) F. C. Frank; J. H. van der Merwe, *Proceedings of the Royal Society of London, Series A*, **198**, 205, **1949**.
- (36) E. Bauer, *Zeitschrift fur Kristallographie*, **110**, 423, **1958**.
- (37) J. H. van der Merwe In *Chemistry and Physics of Solid Surfaces V*; R. Vanselow and R. Howe, Eds.; Springer-Verlag: New York, 1984.

- (38) F. C. Frank; J. H. van der Merwe, Proceedings of the Royal Society of London. Series B, 198, 216, **1949**.
- (39) E. Bauer; H. Poppa, Thin Solid Films, 12, 167, **1972**.
- (40) K. T. Huang; R. M. Cohen; G. B. Stringfellow, Journal of Crystal Growth, 156, 320, **1995**.
- (41) M. A. Berding; M. van Schilfgaarde; A. Sher; M. J. Antonell; C. R. Abernathy, submitted to Journal of Electronic Materials,
- (42) R. E. Honig; D. A. Kramer, RCA Review, 30, 285, **1969**.
- (43) R. E. Honig, RCA Review, 23, 567, **1962**.
- (44) M. B. Panish; R. A. Hamm, Journal of Crystal Growth, 78, 445, **1986**.
- (45) Hazardous Material Control and Management / Hazardous Material Information System Material Safety Data Sheets; Solutions Software Corporation, Orlando, FL.
- (46) M. J. Antonell; C. R. Abernathy, Proceedings of the Materials Research Society, 379, 511, **1995**.
- (47) Joint Committee on Powder Diffraction Standards Mineral Powder Diffraction File; JCPDS International Centre for Diffraction Data: Swarthmore, PA, 1980.
- (48) V. Krishnamoorthy, Ph. D. Dissertation, University of Florida, 1992.
- (49) W. Acree, unpublished 1995.
- (50) Handbook of Auger Electron Spectroscopy; C. L. Hedberg, Ed.; Physical Electronics, Inc.: Eden Prairie, MN, 1995.
- (51) M. Razeghi; J. Kim; E. Michel; J. Xu, Contract Report, 1997.
- (52) H. Asahi; K. Yamamoto; K. Iwata; S. Gonda; K. Oe, Japanese Journal of Applied Physics. 35, L876, **1996**.
- (53) H. Asahi; M. Fushida; K. Yamamoto; K. Iwata; H. Koh; K. Asami; S. Gonda; K. Oe, submitted to Journal of Crystal Growth, **1997**.
- (54) M. Hansen Der Aufbau der Zweistofflegierungen; Springer-Verlag: Berlin, 1936.
- (55) E. Montignie, Bull. Soc. Chim. Franc, 4, 295, **1937**.
- (56) Binary Alloy Phase Diagrams; R. B. Massalski, Ed.; American Society of Metals: 1986; Vol. 2.
- (57) A. Sher, unpublished 1996.
- (58) S. Sekito, Zeitschrift fur Kristallographie, 74, 189, **1930**.
- (59) F. R. Morrel; A. Westgren, Svensk Kem. Tidskr., 46, 153, **1934**.


- (60) N. H. Karam; R. Sudharsanan; T. Parados; M. A. Dodd, preprint, **1997**.
- (61) F. A. Carey Advanced Organic Chemistry; 3rd. ed.; Plenum Press: New York, 1990.
- (62) R. W. Gedridge; C. R. Abernathy, unpublished 1995.
- (63) R. W. Gedridge, unpublished 1995.
- (64) E. A. Beam III; H. F. Chau, Journal of Crystal Growth, 164, 389, **1996**.
- (65) M. Weyers; J. Musolf; D. Marx; A. Kohl; P. Balk, Journal of Crystal Growth, 105, 383, **1990**.
- (66) A. R. Clawson; T. T. Vu; D. I. Elder, Journal of Crystal Growth, 83, 211, **1987**.
- (67) C. C. Hsu; J. S. Yuan; R. M. Cohen; G. B. Stringfellow, Journal of Crystal Growth, 74, 535, **1986**.
- (68) R. W. Gedridge; L. P. Sadwick; G. B. Stringfellow; C. R. Abernathy In International Conference on Chemical Beam Epitaxy and Related Growth Techniques; San Diego, 1995.
- (69) M. J. Antonelli; C. R. Abernathy; R. W. Gedridge, Journal of Crystal Growth, 164, 420, **1996**.
- (70) R. Bhat; J. R. Haynes; H. Schumacker; M. A. Koza; D. M. Hwang; M. H. Meynadier, Journal of Crystal Growth, 93, 919, **1988**.
- (71) E. Byrne In InP and Related Materials; A. Katz, Ed.; Artech House: 1994.
- (72) C. R. Abernathy; P. W. Wisk; S. J. Pearton; F. Ren, Applied Physics Letters, 30, 1184, **1994**.
- (73) Y. M. Cheng; M. Stavola; C. R. Abernathy; S. J. Pearton; W. S. Hobson, Physical Review B, 49, 2469, **1994**.
- (74) B. H. Cheong; K. J. Chang, Physical Review B, 49, 17436, **1994**.
- (75) S. A. Stockman; G. E. Stillman In International Symposium on InP and Related Compounds; Newport, 1992.
- (76) M. L. Timmons; P. K. Chiang; S. V. Hattangady, Journal of Crystal Growth, 77, 37, **1986**.
- (77) M. Rask; G. Landgren; S. G. Anderson; A. Lundberg, Journal of Electronic Materials, 17, 4, **1988**.
- (78) T. J. deLyon; J. M. Woodall; P. D. Kirchner; D. T. MacInturff; G. J. Scilla; F. Cardone, Journal of Vacuum Science and Technology, B9, 136, **1991**.
- (79) Y. M. Houn; S. D. Lester; D. E. Mars; J. N. Miller, Journal of Vacuum Science and Technology, B11, 915, **1993**.

- (80) C. Palmstrom; B. P. Van der Gaag; J. I. Song; S. A. Schwarz In ICCBE-4; Nara, Japan, 1993.
- (81) K. Oe; S. Ando; K. Sugiyama, Japanese Journal of Applied Physics, 20, L303, **1981**.
- (82) T. P. Chin; P. D. Kirchner; J. M. Woodall; C. W. Tu, Applied Physics Letters, 59, 2865, **1991**.
- (83) T. Yamada, Journal of Crystal Growth, 95, 145, **1995**.
- (84) J. M. van Hove; P. P. Chow; M. F. Rosamond; G. L. Carpenter; L. A. Chow, Journal of Vacuum Science and Technology, B12, 1200, **1994**.
- (85) C. R. Abernathy; J. D. MacKenzie; W. S. Hobson; P. W. Wisk, Applied Physics Letters, 65, 2205, **1994**.
- (86) M. Spencer, Presented at Fall Meeting of the Materials Research Society; Boston, MA, 1995.
- (87) C. R. Abernathy; J. D. MacKenzie; S. J. Pearton; W. S. Hobson, Applied Physics Letters, 66, 1969, **1995**.
- (88) W. Schoenfeld; M. J. Antonelli; J. Choi; C. R. Abernathy, submitted to the Journal of the Electrochemical Society.
- (89) C. R. Abernathy; J. D. MacKenzie; S. R. Bharatan; K. S. Jones; S. J. Pearton, Applied Physics Letters, 66, 1632, **1995**.


BIOGRAPHICAL SKETCH

Michael J. Antonell is the sixth child of George and Etta Antonell and was born in Warren, Ohio, in July, 1969. He attended the Howland School System in Howland, Ohio, where he received his primary and secondary education. He then enrolled at Youngstown State University in Youngstown, Ohio, where he obtained a Bachelor of Engineering in 1992. Upon graduation at Youngstown State University he was selected Outstanding Engineering Graduate for the School of Engineering. He proceeded to the University of Florida where he received his master's degree under the tutelage of Professor Kevin S. Jones in the Department of Materials Science and Engineering in August of 1994. From August 1994 until August 1997, Michael worked towards his Ph.D. on the synthesis of Tl-containing III-V materials under the supervision of Cammy R. Abernathy.


I certify that I have read this study and that in my opinion it conforms to acceptable standards of scholarly presentation and is fully adequate, in scope and quality, as a dissertation for the degree of Doctor of Philosophy.


Cammy R. Abernathy, Chairperson
Professor of Materials
Science and Engineering


I certify that I have read this study and that in my opinion it conforms to acceptable standards of scholarly presentation and is fully adequate, in scope and quality, as a dissertation for the degree of Doctor of Philosophy.


Stanley R. Bates
Associate Professor of Materials
Science and Engineering

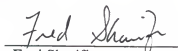
I certify that I have read this study and that in my opinion it conforms to acceptable standards of scholarly presentation and is fully adequate, in scope and quality, as a dissertation for the degree of Doctor of Philosophy.


Kevin S. Jones
Associate Professor of Materials
Science and Engineering

I certify that I have read this study and that in my opinion it conforms to acceptable standards of scholarly presentation and is fully adequate, in scope and quality, as a dissertation for the degree of Doctor of Philosophy.


Steve J. Pearton
Professor of Materials
Science and Engineering

I certify that I have read this study and that in my opinion it conforms to acceptable standards of scholarly presentation and is fully adequate, in scope and quality, as a dissertation for the degree of Doctor of Philosophy.


Fred Sharifi
Assistant Professor of Physics

This dissertation was submitted to the Graduate Faculty of the College of Engineering and to the Graduate School and was accepted as partial fulfillment of the requirements for the degree of Doctor of Philosophy.

August, 1997



Winfred M. Phillips
Dean, College of Engineering

Karen A. Holbrook
Dean, Graduate School